NONLOCAL SOLITONS IN PHOTOREFRACTIVE MATERIALS

by

Jennifer Pauline Ogilvie

B.Sc., University of Waterloo, 1994

A THESIS SUBMITTED IN PARTIAL FULFILLMENT
OF THE REQUIREMENTS FOR THE DEGREE OF
MASTER OF SCIENCE
in the Department
of
Physics

SIMON FRASER UNIVERSITY
August 1996

ISBN 0-612-17036-5

PARTIAL COPYRIGHT LICENSE

I hereby grant to Simon Fraser University the right to lend my thesis, project or extended essay (the title of which is shown below) to users of the Simon Fraser University Library, and to make partial or single copies only for such users or in response to a request from the library of any other university, or other educational institution, on its own behalf or for one of its users. I further agree that permission for multiple copying of this work for scholarly purposes may be granted by me or the Dean of Graduate Studies. It is understood that copying or publication of this work for financial gain shall not be allowed without my written permission.

Title of Thesis/Project/Extended Essay

Nonlocal Solitons in Photorefractive Materials

Author:
(signature)

Jennifer Ogilvie
(name)

Aug 12/1996
(date)

APPROVAL

Name: Jennifer P. Ogilvie

Degree: Master of Science

Title of thesis: Nonlocal Solitons in Photorefractive Materials

Examining Committee: Dr. M. Plischke
Chair

Dr. R.H. Enns
Senior Supervisor

Dr. J. Bechhoefer

Dr. B. Frisken

Dr. S.S. Rangnekar

Dr. K. Rieckhoff
Internal Examiner

Date Approved: 6 August 1996

Abstract

Optical spatial solitons have been the subject of intense theoretical and experimental research in the last thirty years. Spatial solitons have been studied extensively in Kerr media, where they arise when a nonlinear change in refractive index provides a confining effect that compensates for the defocusing effect of diffraction. In 1992 Segev *et al.* [1] predicted that spatial solitons could also occur in photorefractive materials as a result of a similar balance between diffraction and nonlinear photorefractive self-focusing. This was verified experimentally in 1993 by Duree *et al.* [2]. Since then it has been demonstrated that three distinct classes of spatial solitons can exist in photorefractive materials. The first class arises from the nonlocal photorefractive effect and can be generated at extremely low intensities (mW/cm^2). These solitons require the application of an external voltage to the photorefractive crystal and are referred to as nonlocal solitons. The second class is the photovoltaic soliton, which arises in a particular type of photorefractive crystal [3]. The final class of spatial soliton is the screening soliton, which requires similar conditions to the nonlocal one, but is the result of a local change in the index of refraction when the electric field of the optical beam is comparable to the external bias field.

Both bright and dark solitons have been observed experimentally for the three soliton classes. The theories developed for the screening solitons and the photovoltaic solitons account for these observations. However, the theory proposed by Segev *et al.* fails to explain the existence of dark solitons [1]. This thesis examines the assumptions made by Segev *et al.* in an attempt to posit a more general theory that accounts for dark solitons. This requires an understanding of the Kukhtarev-Vinetskii model of photorefraction, and an application of the model to describe the coupling of two spatial modes in photorefractive media. Within the two-wave mixing approximation an equation is derived for the propagation of optical beams in photorefractive materials. The soliton solutions to the equation are studied and

it is shown that the modified theory admits both bright and dark soliton solutions under conditions consistent with experiment. The thesis concludes with an argument that accounts for the stability of these solutions.

Acknowledgements

Thanks to Daniel and to my parents who patiently listened to my tirade of self-doubt.

Suresh and Yves, Daniel and Sandy: thanks for proof-reading my manuscript. Suresh, thank-you for your confidence and our discussion of diffraction. Yves, the pre-defence grilling session was much appreciated.

Thanks to my housemates Ralph and Marc for a fun year of unsolvable puzzles, ginger-bread houses, berry-picking and paper-making.

Thanks to my research group: Darran Edmundson, Richard Enns, Sandra Eix and Sada Rangnekar for their helpful suggestions at group meetings and to Richard for financial support.

In its effect the light was choral. Harmonies of power simultaneously achieved, a depth of light, not one note but many, notes of light sung together. In its high register, far beyond the ears of man, the music of the spheres, vibrated light noted in its own frequency. Light seen and heard. Light that writes on tablets of stone. Light that glories what it touches. Solemn, self-delighting light.

- Jeanette Winterson, *Art & Lies* (1994)

Contents

List of Tables

List of Figures

Chapter 1

Introduction

1.1 The history of the soliton

The first documented observation of a soliton was made by a Scottish engineer named John Scott Russell in 1834 while he was riding on horseback along the Union Canal that connects Edinburgh and Glasgow. He recorded his observation in the following delightful words:

I was observing the motion of a boat which was rapidly drawn along a narrow channel by a pair of horses, when the boat suddenly stopped-not so the mass of water in the channel which it had put in motion; it accumulated round the prow of the vessel in a state of violent agitation, then suddenly leaving it behind rolled forward with great velocity, assuming the form of a large solitary elevation, a rounded, smooth and well-defined heap of water, which continued its course along the channel apparently without change of form or dimunition of speed. I followed it on horseback, and overtook it still rolling on at a rate of some eight or nine miles an hour, preserving its original figure some thirty feet long and a foot to a foot and a half in height. Its height gradually diminished, and after a chase of one or two miles I lost it in the windings of the channel. Such, in the month of August 1834, was my first chance interview with that singular and beautiful phenomenon which I have called the Wave of Translation, ...[6]

Russell's chance encounter with the *Wave of Translation* prompted intense debate because its existence contradicted the shallow wave theory that was well accepted at the time [6]. The controversy was resolved independently by Bo' ,sinesq in 1871 and Lord Rayleigh in 1876 who both recognized the importance of the previously neglected concept of dispersion. They were the first to realize that the solitary wave was a product of the balance between two competing effects: the nonlinear effect, which describes why the crest of a wave moves faster than the rest, and the dispersive effect, which describes the dependence of the wave velocity on the frequency of the wave [7]. They reasoned that the tendency for the wave to 'break' was balanced by the spreading effect of dispersion.

In 1895 Korteweg and de Vries attempted to mathematically describe wave propagation in shallow water, incorporating the effects of dispersion and surface tension. Their efforts resulted in the celebrated KdV equation, which was shown to have solutions much like Russell's solitary wave.

In the years following, the solitary wave was thought to be an unimportant mathematical curiosity of nonlinear wave theory. However, in 1955 it reappeared in a completely different context. At the time, three scientists named Fermi, Pasta and Ulam, were studying the transfer of heat in solids. It was known that a model consisting of a one-dimensional lattice of identical masses connected by linear springs was not sufficient to achieve equipartition of energy among the different modes of the lattice. In other words, a lattice with only harmonic interactions would never reach thermal equilibrium. Debye had suggested that this problem would likely be resolved by including nonlinear interactions between the atoms [6]. Fermi, Pasta and Ulam proceeded to test this hypothesis numerically. They found that the system did not reach thermal equilibrium. Instead, if they initially excited one mode of the lattice, the energy returned almost periodically to this mode and a few nearby ones.

The unexpected results of Fermi, Pasta and Ulam motivated Zabusky and Kruskal to study the problem in greater detail. They were led by a continuum approximation to the KdV equation for describing the energy transfer among the lattice modes. Numerical

simulations of the KdV equation showed that robust pulse-like waves propagated in the system. These solitary waves could pass through each other while maintaining their speed and shape. Zabusky and Kruskal named these waves *solitons* to emphasize their particle-like qualities. In an attempt to explain the Fermi, Pasta and Ulam results, Zabusky and Kruskal launched a sinusoidal pulse on a ring of atoms (see Figure 1.1) [6]. They found that the system evolved to a state in which a number of solitons propagated along the ring with different velocities. Collisions among these solitons caused small phase changes in each soliton. After a long enough time the solitons were observed to collide simultaneously. At this instant the system resembled the initial state. This explained the recurrence seen by Fermi, Pasta and Ulam.

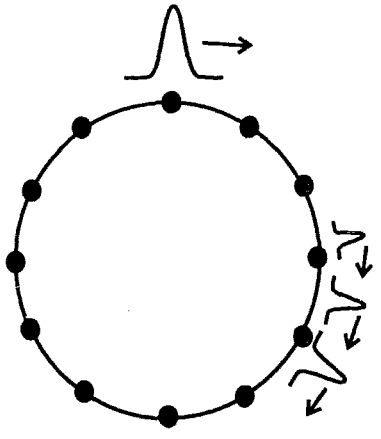

Figure 1.1: Breaking of initial state into solitons. The recurrence of the inital state occurs when the solitons collide simultaneously [6].

In 1967 Gardner *et al.* showed that under some conditions, analytic solutions to the KdV equation could be obtained using what is now called the *inverse scattering method* [8]. They showed that the number of solitons that evolved was dependent on the initial state. Their results were in general agreement with Zabusky and Kruskal's numerical studies.

It is now apparent that solitons are ever-present in our modelling of the physical world. In the past thirty years approximately one hundred different types of nonlinear partial

differential equations have been shown to have soliton or soliton-like solutions [7]. Solitons have appeared in problems as diverse as the biological modelling of protein transport [9] and the atmospheric modelling of Jupiter's long-lasting 'Red Spot' [10].

Perhaps the most widely studied solitons have been optical solitons because of their promising applications. These solitons arise from a balance between dispersion and a nonlinear effect such as the Kerr effect. They have been used successfully to transmit binary data down optical fibers using a scheme where a soliton represents a logical '1' and the absence of a soliton represents a '0'. Optical logic gates using optical solitons have been proposed [11] but have not yet been achieved experimentally.

The definition of a soliton has generated heavy debate. The original definition required it to be 'a localized solution to an exactly integrable partial differential equation that is stable against collisions with other solitons'. In much of the literature a looser definition has been adopted to include all solutions that are *relatively stable* solitary waves. Because many nonlinear partial differential equations are not exactly integrable, solitons are often found numerically. The term relatively stable has come to mean that, numerically, the solutions propagate without changing their shape, and retain their properties upon colliding with other solitons.

1.2 Photorefractive spatial solitons

The Wave of Translation seen by Russell and the other solitons mentioned thus far have been *temporal solitons*, a name given to reflect their unchanging nature as they propagate in time. The solitons that will be studied here are *spatial solitons* that occur in photorefractive crystals such as strontium barium niobate (SBN). They are the spatial analogues of the temporal soliton: the propagation direction plays the role that time plays for a temporal soliton. In the temporal case, dispersion acts to spread the pulse in time, while in the spatial case, diffraction acts to spread the pulse in space. The basic effect of spatial soliton

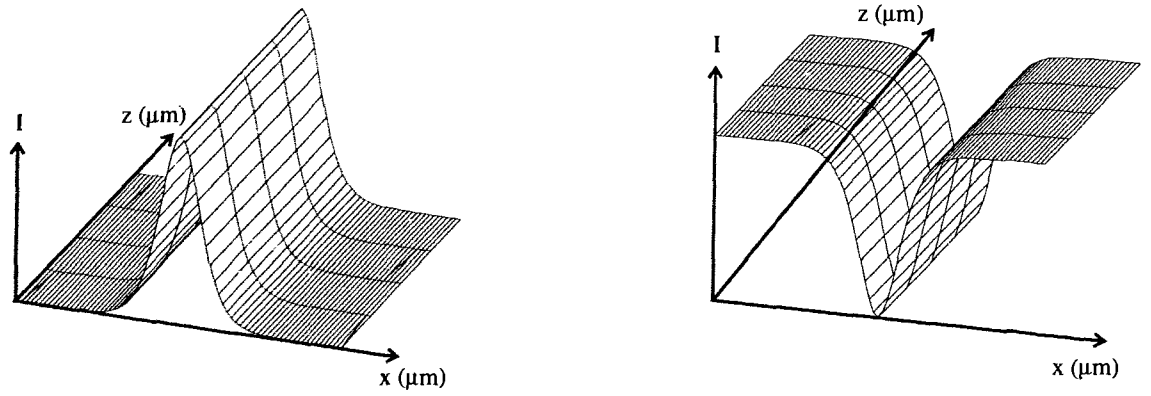

Figure 1.2: The intensity profiles of a) a bright spatial soliton, and b) a dark spatial soliton. The intensity profiles remain unchanged along the propagation direction z.

formation can be explained as follows: when an optical beam enters a photorefractive crystal it spreads via diffraction. In order to form a soliton, this spreading must be balanced by a nonlinear effect. The nonlinearity arises because photorefractive materials undergo a change in index of refraction δn upon illumination. The index change causes a coupling between the spatial modes of the input beam [12]. This coupling results in energy exchange and/or self-phase modulation, depending on the nature of δn. When $\delta n > 0$ the medium is called self-focusing and phase coupling causes the phase of each spatial mode to decrease linearly along the propagation direction. Conversely, when $\delta n < 0$ the medium is self-defocusing. Phase coupling then leads to a linear accumulation of phase in each mode. If δn is imaginary, then energy coupling occurs, causing the amplification of either the low or the high order spatial modes of the input beam. Because diffraction can be considered a linear accumulation of phase, balancing it requires phase coupling rather than energy exchange. Thus a bright soliton can be attained when the medium is self-focusing: the linear decrease in phase due to phase coupling balances the linear increase in phase from diffraction. In contrast, dark

solitons can be attained when the medium is self-defocusing: the linear increase in phase due to phase coupling exactly balances the linear decrease in phase due to diffraction (see Figure 1.3).

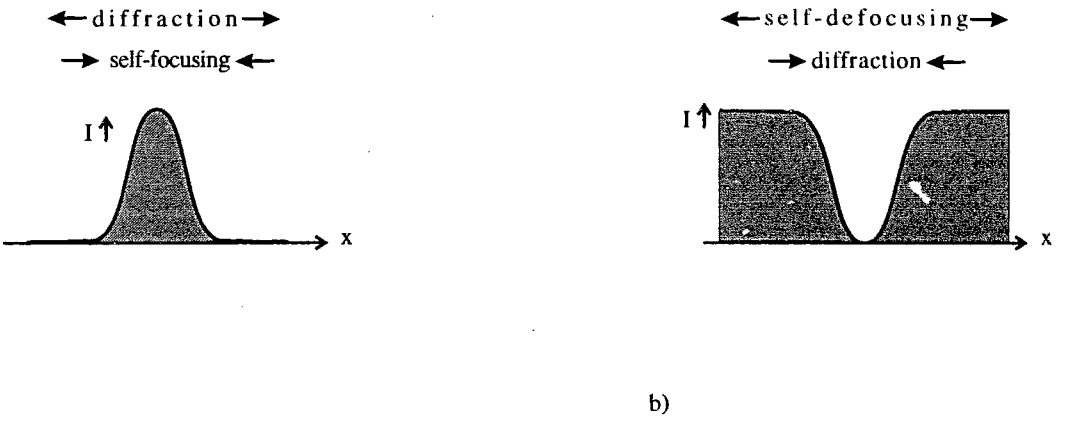

Figure 1.3: a) Intensity profile of a bright soliton ($\delta n > 0$). The spreading effect of diffraction is balanced by self-focusing. b) Intensity profile of a dark soliton ($\delta n < 0$). The inward spread of diffraction is balanced by self-defocusing.

In 1992, Segev *et al.* [1] derived an approximate equation for the propagation of optical beams in photorefractive materials and showed that the equation had bright spatial soliton solutions. These solitons were studied in greater detail by Crosignani *et al.* [5] who found additional analytic solutions and studied their stability and dimensionality [13][14]. These solitons arise from the nonlocal photorefractive effect, and for that reason will be referred to as *nonlocal solitons.* Their formation requires the presence of a bias field, and the magnitude of the bias field must be large compared to the electric field of the incident light. Observation of these bright solitons came in 1993 [2], followed by the experimental discovery of nonlocal dark solitons in 1994 [15]. The theory developed by Segev *et al.* does not account for dark solitons [1][5]. There has been great interest in these solitons because they can be generated at low light intensities, making them better candidates for optical switching

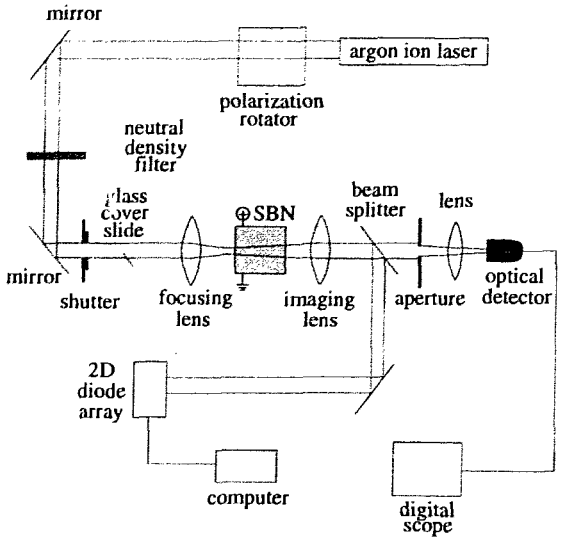

Figure 1.4: The experimental apparatus used in [2] to study nonlocal solitons in SBN. The glass cover slide is inserted for dark solitons only. It is used to obtain the necessary π phase jump at the beam centre. The digital scope monitors the screening of the bias field.

devices than the conventional Kerr solitons. Nonlocal solitons have the disadvantage of being short-lived: they have been reported to last for a maximum duration of ≈ 2 s [4]. On optical time-scales this is considered long enough to be potentially useful. The lifetime of nonlocal solitons is limited because the bias field that is essential to their formation becomes screened by thermally generated electrons inside the crystal. Nevertheless, their lifetime is long compared to the time required for their formation ($\approx 1\text{x}10^{-4}$ s) [16]. For this reason they are considered to exist in 'steady-state' conditions during this short time-window.

The experimental apparatus used to generate nonlocal solitons is shown in Figure 1.4. The material used was a 5 mm x 5 mm x 6 mm SBN crystal, oriented with its c-axis perpendicular to the beam propagation direction and parallel to the polarization of the beam. The beam diameter at the entrance face of the crystal was 81 μm along the c-axis. A digital oscilloscope was used to monitor the intensity of the incident beam after passing through the crystal and an exit aperture the size of the original beam. While the intensity remained constant the system was considered to be in steady-state. Different cross-sections of the beam in the crystal were imaged onto the detector array by moving the imaging lens position with respect to the SBN crystal. The glass slide was inserted for dark soliton

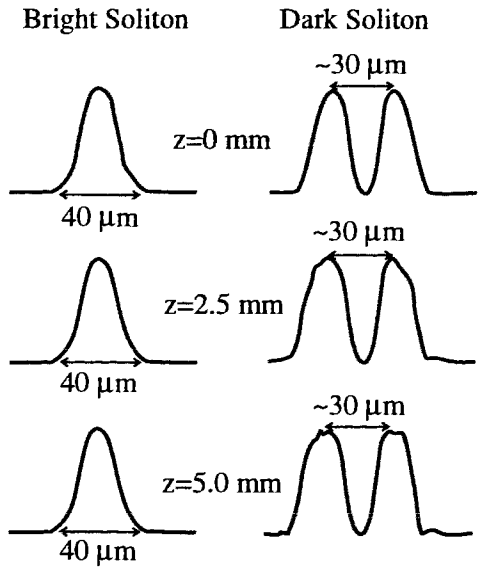

Figure 1.5: Experimental bright and dark soliton profiles in SBN [2][4]. The dark solitons are approximated as a notch out of a gaussian beam. The notch propagates without change in profile.

experiments only. It was tilted to create a π phase shift in half of the beam, yielding an intensity profile with a 'notch' taken out of it. Figure 1.5 shows an example of beam profiles along the c-axis obtained for bright and dark solitons [2][4]. Soliton formation along the other transverse direction has also been observed.

Since the discovery of nonlocal solitons, two other types of photorefractive solitons have been found. One of these is the *photovoltaic soliton*, which occurs in photovoltaic materials such as $LiNbO_3$ [17]. A theory has been developed to account for the existence of both bright and dark photovoltaic solitons, and both types have been observed experimentally [18].

The last photorefractive soliton to be found was the *screening soliton*. It exists under similar conditions to the nonlocal soliton, but requires an external bias field comparable to the electric field of the incident light [19][20]. Screening solitons are formed after the bias field has been nonuniformly screened. The change in index of refraction arises primarily from a local effect that depends on the incident intensity. Screening solitons cannot be generated at intensities as low as their nonlocal counterparts. The theory describing their formation is

reasonably complete and predicts bright and dark spatial solitons, both of which have been observed experimentally [4][21][22].

Many theoretical questions regarding the three soliton types remain unanswered. The theory postulated for all three types is two-dimensional and fails to explain experimentally observed soliton formation in both transverse directions. The evolution properties of photorefractive solitons from arbitrary input beams are also unaccounted for. No studies to date have addressed questions regarding collisions between photorefractive spatial solitons. The theory of nonlocal solitons is the weakest of the three soliton theories because it fails to predict dark solitons.

This thesis tackles the latter problem and modifies the existing nonlocal soliton theory to account for dark soliton solutions. To facilitate this goal the approximations made in [1] and [5] are examined. This requires an understanding of the widely used Kukhtarev-Vinetskii model of photorefraction. The photorefractive nonlinearity for two-wave mixing is developed within the framework of this model and under more general conditions than those outlined in [1] and [5]. Two-wave mixing is studied briefly and the results are extended to provide a description of the propagation of optical beams in photorefractive materials using the two-wave mixing approximation. With this description the search for dark solitons begins.

Chapter 2

Photorefraction

Photorefraction is a process by which the local index of refraction of a medium is changed when it is illuminated by a beam of light with varying spatial intensity [16]. It was discovered in 1966 by Ashkin while he studied the propagation of laser light through $LiNbO_3$. He found that in the region of the laser beam there was a local change in the refractive index which caused the beam wavefront to distort as it passed through the crystal. He considered this an undesirable effect in an otherwise high quality optical crystal, and termed the effect 'optical damage' [23].

Although photorefraction was originally considered a nuisance, the positive attributes of the effect were soon appreciated and a number of applications were proposed. Because of the reversible nature of the refractive index variations, it was clear that these crystals could be used as recyclable photosensitive media. With the recent improvement of doping and crystal growth techniques, it is now feasible to use photorefractive crystals for holography and optical information processing [23].

The physical origin of the photorefractive effect has been of considerable interest to scientists studying solid-state physics, semiconductors, and coherent optics. Since Ashkin's observation, the theory of photorefraction has developed considerably. The current theory is a collaborative effort beginning with work by Chen in 1967, and fleshed out by contributions

from Amodei, Kukhtarev and Vinetskii and others [3].

A qualitative model of photorefraction is as follows: free carriers are produced in the crystal by photoionization and are transported into non-illuminated regions where they become trapped. The resulting charge distribution causes the formation of an internal electric field, which modulates the index of refraction of the material via the linear Pockel's effect.

The aim of this chapter is to present the essentials of the commonly used Kukhtarev-Vinetskii model of photorefraction and to utilize this model in deriving an expression for the change in refractive index when a photorefractive material is illuminated by two plane waves. This result will form the basis of our description of the propagation of optical beams in photorefractive crystals.

2.1 Charge carrier generation

Pure photorefractive crystals are transparent in the visible regime and thus the charge donors and acceptors needed for photorefraction must be provided by impurities [3]. In lithium niobate ($LiNbO_3$), potassium niobate ($KNbO_3$) and most other photorefractive crystals, Fe ion impurities in different valence states act as both the donors and acceptors. The

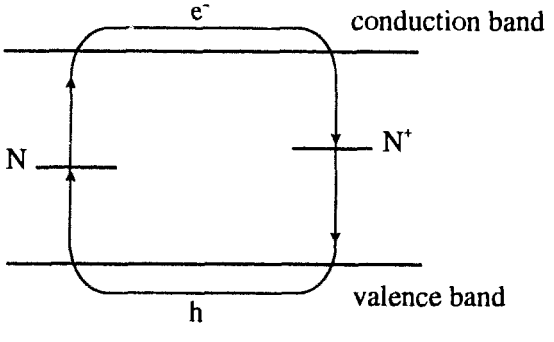

Figure 2.1: Energy level model for photorefraction in which a single type of donor and acceptor species are present, giving rise to electrons in the conduction band and holes in the valence band.

concentrations of impurities can be controlled through doping. Photorefraction has been found to occur for Fe ion concentrations ranging between $10^{16}-10^{19}\text{cm}^{-3}$ [3]. Other common types of impurities include copper, rhodium and manganese. The location of the impurities in the crystal is often unknown. The impurities may substitute for certain cations in the crystal, or occur as some other type of defect [23].

Upon illumination, light is absorbed by an acceptor and ionization occurs, promoting an electron into the conduction band and leaving a hole in the valence band as shown in Figure 2.1. After ionization, the electron is free to move in the conduction band until it recombines with an acceptor elsewhere in the crystal. Although hole conduction occurs, it will be neglected in the analysis that follows because the mobility of the holes is small compared to the electron mobility. Thus hole conduction makes a negligible contribution to photorefraction under most conditions [23]. In ferroelectric crystals, it is typically Fe^{2+} ions that act as the donors and Fe^{3+} ions that act as the acceptors. The photoexcitation energy for Fe doped ferroelectric crystals ranges between $3.1 - 3.2$ eV.

2.2 Transport of charge carriers

Once the charge carriers have been generated, they are transported out of the illuminated regions of the crystal by three mechanisms: diffusion, drift and the photovoltaic effect.

Diffusion transport occurs because the electrons migrate from the illuminated regions, where their concentration is high, into dark areas where their concentration is low. Figure 2.2 shows the diffusion field created by an incident intensity with a sinusoidal modulation. The charge carriers typically travel a distance L_d before being re-trapped. This distance depends largely on the acceptor concentration and charge mobility. Note that the space-charge field E_{sc} created by the charge distribution is $\pi/2$ out of phase with the incident intensity.

Drift transport occurs when an external electric field E_0 is applied to the crystal. This

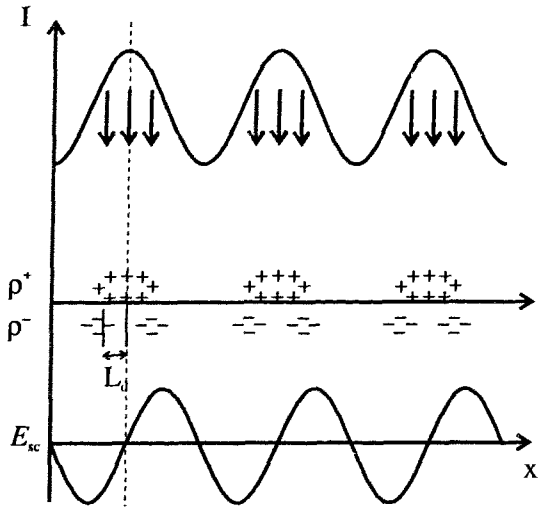

Figure 2.2: Charge transport via diffusion. The positive charge distribution ρ^+ is a result of ionized donors that are left in high illumination regions when the carrier electrons diffuse to regions of low electron concentration. The resulting internal field E_{sc} is shifted by $\pi/2$ with respect to the incident illumination. [23].

field causes unidirectional electron transport away from illuminated areas as shown in Figure 2.3. Electrons typically move a distance L_0 before becoming re-trapped. If L_0 is small compared to the wavelength of the intensity modulation, then the space-charge field E_{sc} created by the redistribution of charge will be almost in phase with the incident intensity.

Photorefractive materials are often ferroelectric, meaning that at some temperatures they possess a spontaneous polarization [24]. Thus the conduction electrons move preferentially along the direction of this polarization. Charge transport of this type is called photovoltaic and will not be included in the analysis that follows because it is generally negligible in the materials used for studying nonlocal solitons [23]. For information regarding soliton formation under conditions where photovoltaic transport is important, the interested reader is referred to [17].

The transport of charge carriers in the crystal results in a nonuniform charge distribution which in turn creates an internal electric field. Because the charge distribution in one part of the crystal gives rise to the electric field in another part of the crystal, the photorefractive effect is said to be a nonlocal effect. The length scale over which this nonlocal effect acts depends on the mean distance of charge transport (L_0 in the case of drift transport, or L_d

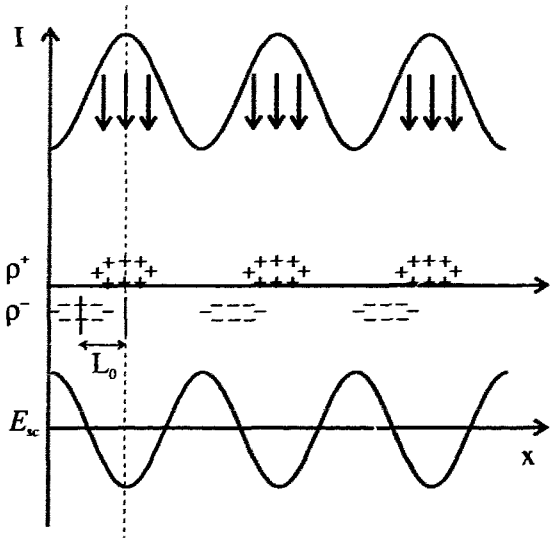

Figure 2.3: Charge transport via drift. The positive charge distribution ρ^+ is a result of ionized donors that are left in high illumination regions when the carrier electrons drift to low illumination areas of the crystal. The resulting internal field E_{sc} is almost in phase with the incident illumination [23].

if transport is by diffusion).

2.3 Formation of the space-charge field

To derive an expression for the index of refraction change, it is necessary to quantify the electric field formed by the charge distribution in the crystal. To do this we will make several simplifying assumptions: i) we neglect the photovoltaic effect, ii) we neglect absorption and ii) we assume that the intensity modulation is small.

With these assumptions in mind let us begin by defining N_D as the total number density of dopants in the material, and N^+ and N as the acceptor and donor number densities such that $N_D = N + N^+$. The rate of electron generation is then $(sI + D)N$, where s is the cross-section of photoionization, and D is the rate of thermal generation of electrons. The rate of trap capture is given by $\Gamma\rho N^+$ where Γ is the recombination coefficient and ρ is the number density of the electrons. Thus the rate equation for the number density of acceptors is given by

$$\frac{\partial N^+}{\partial t} = (sI + D)N - \Gamma\rho N^+ \tag{2.1}$$

Notice that we have neglected the decrease in intensity due to absorption. This approximation holds well for thin crystals but becomes worse as the distance the beam travels in the photorefractive media increases.

The rate of generation of electrons is the same as that of the ionized impurities, except that the electrons are mobile while the acceptors are fixed in the crystal. Thus the rate equation for the electron number density can be written as

$$\frac{\partial}{\partial t}(\rho - N^+) = \nabla \cdot \frac{\mathbf{j}}{\mathrm{e}} \tag{2.2}$$

The electron current, which is given by

$$\mathbf{j} = \mathrm{e}\mu\rho\mathbf{E} + \mathrm{k_b T}\mu\nabla\rho \tag{2.3}$$

arises from charge transport contributions from drift and diffusion respectively. Here μ is the electron mobility, e is the electron charge, and $\mathrm{k_b}$ is Boltzmann's constant. Finally, Poisson's equation gives an expression for the electric field

$$\nabla \cdot \epsilon\mathbf{E} = -\mathrm{e}(\rho + N_A - N^+) \tag{2.4}$$

where N_A is the number density of negative ions that are necessary to preserve charge neutrality in the crystal. In the absence of illumination, the charge neutrality condition can be expressed as $(\rho + N_A - N^+) = 0$.

A general solution to these equations is not available. However, for reasons that will become apparent, we are interested in the solution for an incident intensity of two plane waves of the same frequency but different wavevectors.

2.4 The space-charge field from two plane waves

Consider the incidence of two plane waves of the same frequency ω onto a photorefractive crystal. The electric field can be written as

$$\mathbf{E} = a_1 e^{i(\mathbf{q}_1 \cdot \mathbf{r} - \omega t)} \hat{\mathbf{e}}_1 + a_2 e^{i(\mathbf{q}_2 \cdot \mathbf{r} - \omega t)} \hat{\mathbf{e}}_2 \tag{2.5}$$

If the polarizations of the two plane waves are not orthogonal, they will form an interference pattern, or grating, with an intensity given by

$$\begin{aligned} I(\mathbf{r}) &= \mathbf{E} \cdot \mathbf{E}^* \\ &= I_0 + Re(I_1 e^{i\mathbf{K} \cdot \mathbf{r}}) \end{aligned} \tag{2.6}$$

where

$$\begin{aligned} I_0 &= |a_1|^2 + |a_2|^2 \\ I_1 &= 2a_1^* a_2 \hat{\mathbf{e}}_1 \cdot \hat{\mathbf{e}}_2 \end{aligned} \tag{2.7}$$

and $\mathbf{K} = \mathbf{q}_2 - \mathbf{q}_1$ which is related to the spacing of the grating Λ by $K = 2\pi/\Lambda$.

This provides the motivation for the approximation that we will use to solve the rate equations for the space-charge field in the crystal. If the intensity varies according to Eq. (2.6), it is reasonable to assume that, to a first approximation, the equations for the electron density and the space-charge field will have a similar form. The justification for this is simply that we expect the charge distribution and thus the space-charge field to reflect the spatial variation of the incident light. This has been shown rigorously by Kukhtarev to hold for the fundamental Fourier component of the input intensity [25][26]. Higher order harmonics with spatial frequencies $2\mathbf{K}, 3\mathbf{K}...$ become important as $I_1/(I_0 + I_d) \rightarrow 1$. Here $I_d = D/s$ is the 'dark irradiance' which is the equivalent irradiance that accounts

for the electrons produced due to thermal effects. Moharam *et al.* have shown that for $I_1/(I_0 + I_d) = 0.9$ only the fundamental Fourier component contributes [27]. Thus we will assume $I_1/(I_0 + I_d) \ll 1$ which is often called the small modulation approximation. Physically, it corresponds to ensuring that the background illumination of the crystal is large enough to guarantee high conductivity in all regions of the crystal.

With these approximations we write

$$\begin{aligned} \mathbf{E} &= \mathbf{E}_0 + \mathbf{E}_{sc} \\ &= \mathbf{E}_0 + Re(\mathbf{E}_1 e^{i\mathbf{K}\cdot\mathbf{r}}) \\ \rho &= \rho_0 + Re(\rho_1 e^{i\mathbf{K}\cdot\mathbf{r}}) \end{aligned} \tag{2.8}$$

where E_0 is the external field applied to the crystal. We are now in a position to solve the rate equations for the two plane wave case.

Solution of these equations proceeds by eliminating $\mathbf{j}, N$ and N^+ to obtain equations involving ρ and $\mathbf{E}$.

For the zeroth order in the electron density we obtain:

$$\rho_0 = (sI_0 + D)\frac{(N_D - N_A - \rho_0)}{\Gamma(N_A + \rho_0)} \approx \frac{(sI_0 + D)(N_D - N_A)}{\Gamma N_A} \tag{2.9}$$

The final expression for ρ_0 has been derived based on the assumption that $|\rho_0| \ll |N_D - N_A|$ and $|\rho_0| \ll |N_A|$. This assumption is reasonable because typical lasers have irradiances less than 1 W/cm^2, and for most photorefractive crystals the absorption coefficient is less than 1 cm^{-1} and the recombination time less than 1 μs. This leads to electron number densities of $10^9 - 10^{12}$ cm^{-3}, which are significantly lower than the typical number densities for the impurities, which are usually of the order $10^{16} - 10^{17}$ cm^{-3}.

To simplify the notation in the solution of the first order quantities, it is useful to define the following rate constants:

$$\Gamma_{di} = \frac{e\mu\rho_0}{\epsilon_o\epsilon} \quad (2.10)$$

$$\Gamma_I = sI_0 + D + \Gamma\rho_0 \quad (2.11)$$

$$\Gamma_R = \Gamma(N_A + \rho_0) \quad (2.12)$$

$$\Gamma_E = K\mu E_0 \quad (2.13)$$

$$\Gamma_D = \frac{K^2 k_b T\mu}{e} \quad (2.14)$$

where Γ_{di} is the dielelectric relaxation rate, Γ_I is the sum of ion production and recombination rates, Γ_R is the electron recombination rate, Γ_E is the mean field drift rate and Γ_D is the diffusion rate.

These definitions lead to the following equations in the first order terms ρ_1 and E_1:

$$\begin{aligned}(i\Gamma_E + \Gamma_D + \Gamma_I + \Gamma_R)\rho_1 + (-\Gamma_{di} + \Gamma_I)A_1 &= (N_D - N_A - \rho_0)sI_1 \\ (\Gamma_I + \Gamma_R)\rho_1 + \Gamma_I A_1 &= sI_1(N_D - N_A - \rho_0) \end{aligned} \quad (2.15)$$

where $A_1 = i\epsilon_o\epsilon K E_1/e$.

In the steady state, when $\mathbf{E_0}||\mathbf{K}$, the equations reduce to the following expression for E_1:

$$\begin{aligned} E_1 &= E_q\left[\frac{E_d - iE_0}{E_0 + i(E_d + E_q)}\right]\frac{I_1}{I_0 + I_d} \\ &= E_m\frac{I_1}{I_0 + I_d} \end{aligned} \quad (2.16)$$

where $\mathbf{E_1}||\mathbf{K}$ and

$$\begin{aligned} E_d &= k_b T K/e \\ E_q &= \frac{e}{(\epsilon\epsilon_o K)}N_A(1 - N_A/N_D) \end{aligned}$$

$$E_m = E_q \left[\frac{E_d - iE_0}{E_0 + i(E_d + E_q)} \right] \tag{2.17}$$

Here E_m is a complex mean field, E_d is the diffusion field and E_q is the limiting space-charge field (i.e.-the maximum possible field if all donors were excited). The quantity $N_A(1 - N_A/N_D)$ is the ionized trap density. The dark irradiance I_d is typically small (≈ 10 mW/cm^2) [4], but has been found to be as large as $100 - 1000$ mW/cm^2 in low purity crystals [28]. It is often neglected because it is usually small compared to the incident intensity, however, it makes an important contribution in dark areas if the intensity I_0 is low [5][28]. This does not conflict with the small modulation approximation: we require only that $I_1 \ll (I_0 + I_d)$, not that $(I_0 + I_d)$ be large.

Thus our final expression for the space-charge field E_{sc} is given by

$$E_{sc} = Re\left(\frac{I_1}{I_0 + I_d} E_m e^{i\mathbf{K}\cdot\mathbf{r}} \right) \tag{2.18}$$

2.5 The electro-optic effect

All photorefractive materials are electro-optic crystals, meaning that in the presence of an electric field, the index of refraction is changed via the electro-optic effect. The electro-optic effect is traditionally defined in terms of the impermeability tensor η_{ij}. The change in η_{ij} is given by

$$\Delta\eta_{ij} = \Delta\left(\frac{1}{n^2}\right)_{ij} = r_{ijk}E_k + s_{ijkm}E_kE_m \tag{2.19}$$

where E_k and E_m are components of the electric field. The constant r_{ijk} is an element of the linear electro-optic tensor that accounts for the linear Pockel's effect. The Kerr effect is described by the quadratic electro-optic tensor with components s_{ijkm}. In photorefractive materials, most of the phenomena of interest occur for small electric fields ($\approx 10^4$ V/m) and are therefore a result of the Pockel's effect. The Kerr effect contributes at much higher electric fields ($\approx 10^6$ V/m) and can therefore be neglected.

The linear electro-optic coefficients r_{ijk} are components of a rank 3 tensor. However, the symmetry properties of the impermeability tensor allow the interchange of the indices i and j, which reduces the number of independent components from 27 to 18. As a result, it is convenient to introduce the traditional contracted indices defined by

$$\begin{aligned}
1 &= (11) = (xx) \\
2 &= (22) = (yy) \\
3 &= (33) = (zz) \\
4 &= (23) = (32) = (yz) = (zy) \\
5 &= (31) = (13) = (zx) = (xz) \\
6 &= (12) = (21) = (xy) = (yx)
\end{aligned} \tag{2.20}$$

Using these definitions we can write $r_{Ik} = r_{ijk}$ where I is the contracted index and $k = 1, 2, 3$ or (x,y,z). In this notation the electro-optic coefficients are written in terms of a 6x3 matrix.

In the previous sections we derived the space-charge field in photorefractive crystals for the case of two plane waves present in the medium. With knowledge of the electro-optic tensor, Eq. (2.19) can then be used to compute the change in index induced by this electric field.

The majority of experimental work has used SBN which has the following electro-optic tensor:

$$\begin{bmatrix}
0 & 0 & r_{13} \\
0 & 0 & r_{13} \\
0 & 0 & r_{33} \\
0 & r_{42} & 0 \\
r_{42} & 0 & 0 \\
0 & 0 & 0
\end{bmatrix} \tag{2.21}$$

where the c-axis of the crystal is chosen to lie along the z-direction. SBN belongs to the point

group $4mm$, and has only three nonzero coefficients. At room temperature $r_{33} \gg r_{13},\ r_{42}$.

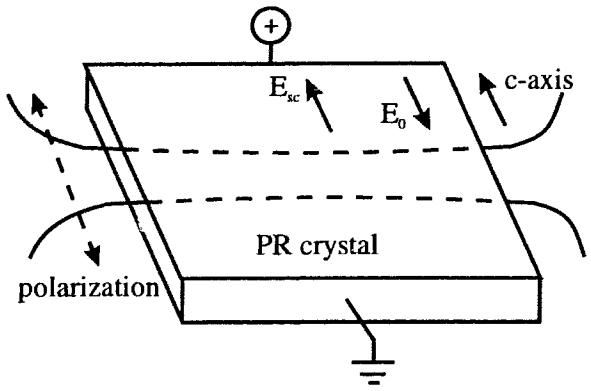

Figure 2.4: Geometry used to compute $\delta n(\mathbf{r}, z)$. The bias field E_0 is applied along the c-axis and the space-charge field E_{sc} forms in the opposite direction as shown.

Using the geometry shown in Figure 2.4 the grating vector K lies parallel to the c-axis of the crystal and the induced space-charge field is along this direction. Therefore the electric field vector can be written as $(0, 0, E_{sc})$, and the components of the impermeability tensor can be determined from Eq. (2.19) and the electro-optic tensor Eq. (2.21). For the two-plane wave case and our specific geometry, we obtain:

$$\Delta\left(\frac{1}{n^2}\right) = \begin{bmatrix} r_{13} & 0 & 0 \\ 0 & r_{13} & 0 \\ 0 & 0 & r_{33} \end{bmatrix} E_{sc} \tag{2.22}$$

One final step remains to determine the change in index of refraction: we need to consider the polarization $\mathbf{p}$ of the incident light. We are interested in the case where the light is polarized along the c-axis (TE polarization). The resulting change in index is computed as follows:

$$\delta n(\mathbf{r}, z) = -\frac{1}{2} n_0^3 \left\langle \Delta\left(\frac{1}{n^2}\right) \right\rangle$$

$$
\begin{aligned}
&= -\frac{1}{2}n_0^3\left\langle \mathbf{p}\left|\Delta\left(\frac{1}{n^2}\right)\right|\mathbf{p}\right\rangle \\
&= -\frac{1}{2}n_0^3 r_{33}E_{sc} \qquad (2.23)
\end{aligned}
$$

where n_0 is the index of refraction in the presence of zero illumination.

SBN has been the material of choice in soliton experiments for several reasons. It can be produced with high purity, and its electro-optic tensor has many zero entries which simplifies the above analysis. The fact that r_{33} is so much larger than the other components also guarantees that for our geometry, δn for the extraordinary polarization is much larger than δn for waves with ordinary polarization. This is important because our description of optical beams in photorefractive materials that will be developed in the upcoming chapter is a two-dimensional one and cannot account for coupling along both transverse coordinates. Thus it is desirable to have dominant coupling along the direction of interest.

We arrive at our final expression for the change in refractive index in the two-plane wave case in SBN by substituting Eq. (2.18) into Eq. (2.23)

$$
\begin{aligned}
\delta n(\mathbf{r},z) &= -\frac{1}{2}n_0^3 r_{33} Re\left(\frac{I_1}{I_0+I_d}E_m e^{i\mathbf{K}\cdot\mathbf{r}}\right) \\
&= \frac{1}{I_0+I_d}\left[\frac{\hat{\delta n}(\mathbf{q}_1,\mathbf{q}_2)}{2}e^{i\mathbf{K}\cdot\mathbf{r}}a_1(z)^* a_2(z) + cc.\right] \qquad (2.24)
\end{aligned}
$$

where

$$
\hat{\delta n}(\mathbf{q}_1,\mathbf{q}_2) = -\frac{1}{2}n_0^3 r_{33}E_m(\mathbf{q}_1,\mathbf{q}_2) \qquad (2.25)
$$

The form of Eq. (2.24) reveals that the change in index of refraction under these conditions arises from coupling between the two plane waves in the medium. When this coupling is small, more complicated intensities can be decomposed into their spatial modes and analyzed in terms of the coupling that occurs between each pair of spatial modes. This is called the *two-wave mixing approximation.*

Thus far we have described the Kukhtarev-Vinetskii model of photorefraction and used

it to derive an expression for $\delta n(\mathbf{r}, z)$ for the specific case of two plane waves in the medium. Our major assumptions have been i) that the photovoltaic effect is negligible, ii) that the intensity decrease due to absorption is small and iii) that the modulation of the intensity pattern is small. In addition we must ensure that the crystal is strongly biased. All of these conditions can be achieved easily in the lab. Our expression for $\delta n(\mathbf{r}, z)$ is similar to the one used by Segev *et al.* [1], with the exception that we have included the dark irradiance term. Our motivation for this is that we expect it to make an important contribution in regions of the crystal where the beam irradiance is small. The results developed here will prove useful when we employ the two-wave mixing approximation in the next chapter to describe the propagation of optical beams in photorefractive materials. We will use this description to look for conditions under which soliton propagation is possible.

Chapter 3

Photorefractive optics

The purpose of this chapter is to develop the necessary equations to describe the propagation of optical beams in photorefractive media. The nonlinear wave equation will be derived, and the photorefractive nonlinearity will be discussed within the framework of the two-wave mixing approximation.

3.1 Two-wave mixing in photorefractive materials

First let us return to the simple two plane wave case. Thus far we have shown that when two plane waves are incident on the photorefractive crystal an index grating is formed, and we have derived an expression for the grating. Because the two plane waves actually create the index grating, they are perfectly phase-matched to it and will undergo Bragg scattering (see Figure 3.1). We will find that this results in coupling between modes, which can cause energy transfer and self-phase modulation.

For simplicity we will assume that the two plane waves are polarized along the same direction. To study the coupling between these modes we substitute the electric field

$$E = a_1 e^{i(\mathbf{q}_1 \cdot \mathbf{r} - \omega t)} + a_2 e^{i(\mathbf{q}_2 \cdot \mathbf{r} - \omega t)} \tag{3.1}$$

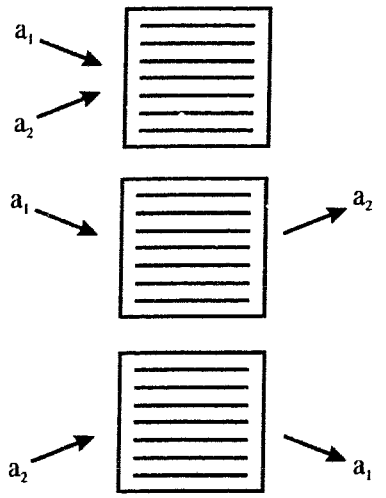

Figure 3.1: Bragg scattering due to an index grating in photorefractive media. Top: A grating is formed by the pair of plane waves a_1 and a_2. Middle: Beam a_1 is diffracted into beam a_2. Bottom: Beam a_2 is diffracted into beam a_1.

into the scalar wave equation

$$\nabla^2 E + \frac{\omega^2}{c^2} n^2 E = 0 \tag{3.2}$$

If we treat the change in refractive index due to the photorefractive effect as a small perturbation and write

$$n = n_0 + \delta n(\mathbf{r}, z) \tag{3.3}$$

where n_0 is the unperturbed index of refraction, then the wave equation becomes:

$$\nabla^2 E + \frac{\omega^2 n_0^2}{c^2} E = -\frac{2\omega^2 n_0 \delta n(\mathbf{r}, z)}{c^2} E \tag{3.4}$$

If both waves propagate in the xz plane and have infinite extent, then a_1 and a_2 are functions of z only. This approximation amounts to neglecting diffraction for the moment and studying only the nonlinear coupling between the modes. Later in our description of optical beams, diffraction will play a key role. We wish to study the steady-state behaviour of a_1 and a_2, so the problem has no time dependence. If we employ the slowly varying envelope

approximation (or paraxial approximation), we can neglect second derivatives in z:

$$\left|\frac{d^2a_j}{dz^2}\right| \ll \left|\beta_{\mathbf{q}_j}\frac{da_j}{dz}\right|, \quad j = 1,2 \tag{3.5}$$

Recalling our previous result for $\delta n(\mathbf{r}, z)$:

$$\delta n(\mathbf{r}, z) = \frac{1}{I_0 + I_d}\left[\hat{\delta n}(\mathbf{q}_1, \mathbf{q}_2)e^{i\mathbf{K}\cdot\mathbf{r}}a_1^*(z)a_2(z) + cc.\right] \tag{3.6}$$

then after grouping terms with the same exponential powers, we obtain the following equations to describe the coupling of the two plane waves

$$\begin{aligned} 2i\beta_{\mathbf{q}_1}\frac{da_1}{dz} &= -\frac{\omega^2 n_0 \hat{\delta n}^*(\mathbf{q}_1, \mathbf{q}_2)}{c^2(I_0 + I_d)}a_2a_2^*a_1 \\ 2i\beta_{\mathbf{q}_2}\frac{da_2}{dz} &= -\frac{\omega^2 n_0 \hat{\delta n}(\mathbf{q}_1, \mathbf{q}_2)}{c^2(I_0 + I_d)}a_1a_1^*a_2 \end{aligned} \tag{3.7}$$

where $\beta_{\mathbf{q}_1}$ and $\beta_{\mathbf{q}_2}$ are the z-components of the wave vectors $\mathbf{q}_1$ and $\mathbf{q}_2$.

If both plane waves are incident on the same side of the crystal, then for simplicity we assume

$$\beta_{\mathbf{q}_1} = \beta_{\mathbf{q}_2} = k\cos(\theta) \tag{3.8}$$

Neglecting loss in the medium, Eq. (3.7) can be written as

$$\begin{aligned} \frac{da_1}{dz} &= \frac{i}{2\cos(\theta)(I_0 + I_d)}\hat{\delta n}(\mathbf{q}_1, \mathbf{q}_2)|a_2|^2a_1 \\ \frac{da_2}{dz} &= \frac{i}{2\cos(\theta)(I_0 + I_d)}\hat{\delta n}(\mathbf{q}_1, \mathbf{q}_2)|a_1|^2a_2 \end{aligned} \tag{3.9}$$

To study the amplitude and phase coupling of the system, it is convenient to rewrite the amplitudes as $a_1 = \sqrt{I_1}e^{-i\Psi_1}$ and $a_2 = \sqrt{I_2}e^{-i\Psi_2}$. In addition, we define the complex

coupling constant

$$\Omega = \nu + i\zeta = i\frac{\pi}{\lambda \cos(\theta)}\hat{\delta n}(\mathbf{q}_1, \mathbf{q}_2) \tag{3.10}$$

Eq. (3.9) then yields two sets of simplified coupled equations, one for the intensities:

$$\begin{aligned} \frac{dI_1}{dz} &= -2\frac{\nu}{I_0 + I_d} I_2 I_1 \\ \frac{dI_2}{dz} &= 2\frac{\nu}{I_0 + I_d} I_1 I_2 \end{aligned} \tag{3.11}$$

and another for the phases of the two plane waves:

$$\begin{aligned} \frac{d\Psi_1}{dz} &= -\frac{\zeta}{I_0 + I_d} I_2 \\ \frac{d\Psi_2}{dz} &= -\frac{\zeta}{I_0 + I_d} I_1 \end{aligned} \tag{3.12}$$

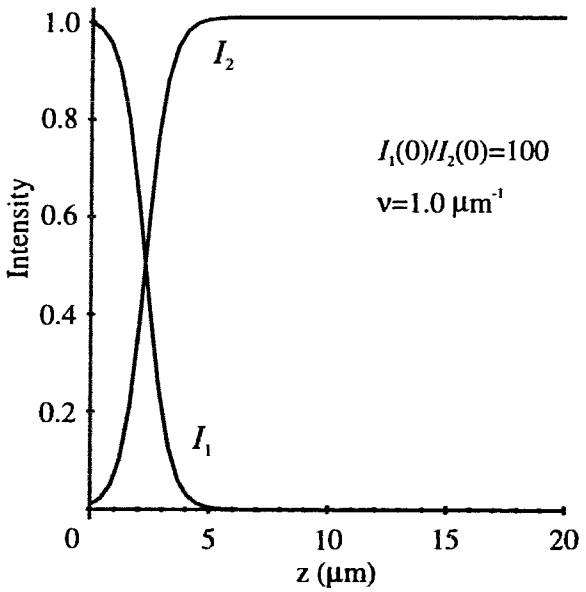

Figure 3.2: Energy coupling between two plane waves: the energy initially in I_1 flows into I_2. Here $\nu = 1.0$ and $\zeta = 0$ which corresponds to an imaginary $\hat{\delta n}(\mathbf{q}_1, \mathbf{q}_2)$. $I_d = I_2(0)$.

Studying this set of coupled equations, one finds that the coupling constant Ω dictates the

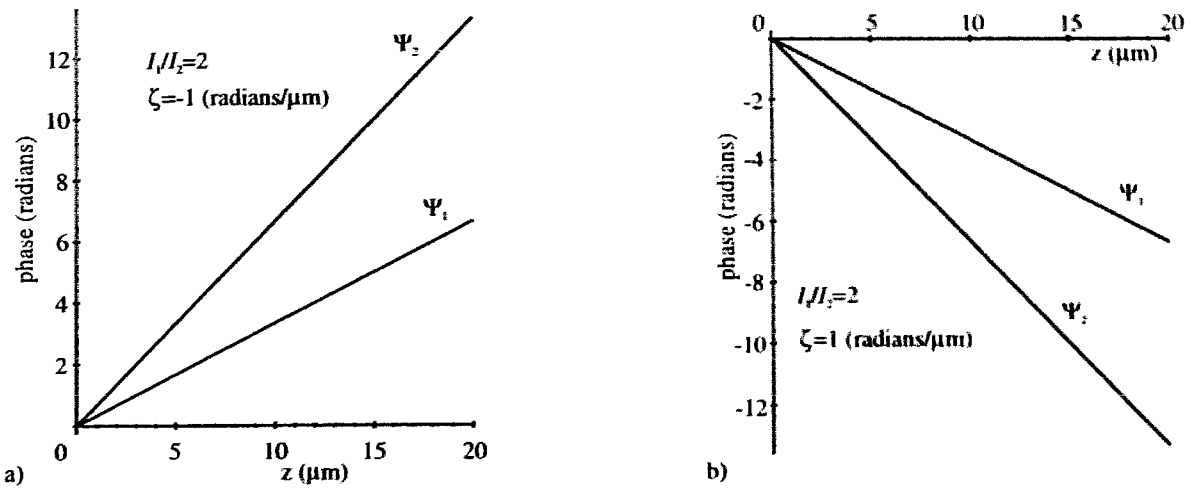

Figure 3.3: Phase coupling between two plane waves: both plane waves change phase in a linear fashion. a) Self-defocusing: $\zeta = -1, \nu = 0$ and the phase of both plane waves increases with z. b) Self-focusing: $\zeta = 1, \nu = 0$ and the phase of both plane waves decreases with z. There is no energy exchange between modes ($\delta\hat{n}(\mathbf{q}_1, \mathbf{q}_2)$ is real).

nature of the interaction between the plane waves. Adding the two equations in Eq. (3.11) reveals that $I_1 + I_2 = constant$. If Ω is real, there is energy exchange between the two modes as shown in Figure 3.2. The direction of energy flow depends on the sign of Ω. If $\Omega > 0$, energy flows from the higher spatial modes into the lower spatial modes. When $\Omega < 0$ the energy flows the other way.

When Ω is purely imaginary there is no energy exchange between the modes, but phase coupling occurs as shown in Figure 3.3. When $\zeta > 0$ the medium is referred to as self-focusing and the phases decrease linearly with propagation distance. Conversely, when $\zeta < 0$ the medium is self-defocusing and the modes accumulate phase linearly.

Thus the nature of Ω determines what type of coupling occurs between spatial modes [16]. If we recall our definition of Ω, given by Eq. (3.10), it is evident that $\delta\hat{n}(\mathbf{q}_1, \mathbf{q}_2)$ determines the character of Ω and therefore of the coupling. If $\delta\hat{n}(\mathbf{q}_1, \mathbf{q}_2)$ is imaginary, which occurs when both the drift and diffusion transport mechanisms contribute, then

energy transfer between modes occurs. If $\hat{\delta n}(\mathbf{q}_1, \mathbf{q}_2)$ is real, there is phase coupling and no energy transfer. These ideas will be important later when we look for conditions under which soliton propagation is possible.

3.2 The two-wave mixing approximation

An optical beam can always be described in terms of the complete basis of plane waves. The two-wave mixing formalism assumes that the change in index of refraction when more than two plane wave components are present can be described as a linear summation of all the possible two-wave interactions in the medium. This assumption has been used successfully in the past to describe photorefractive phenomena such as self-focusing, self-defocusing and beam-fanning [12][29] and will be employed here to describe optical beam propagation in photorefractive materials.

3.3 The nonlinear wave equation

We wish to describe the propagation of a monochromatic optical beam of a given frequency ω and polarization travelling in an arbitrary direction we will call z. Assuming the absence of nonlinear interactions between orthogonal polarizations, we can again use a scalar formulation. However, our beam has transverse structure which prohibits us from neglecting diffraction. The electric field associated with the optical beam can be written as:

$$E(\mathbf{r}, z, t) = \frac{1}{2}\left\{e^{i(kz-\omega t)} \int E(\mathbf{q}, \mathbf{r}) e^{i(\beta_q - k)z} f(\mathbf{q}, z) d\mathbf{q} + c.c\right\} \tag{3.13}$$

$$= \frac{1}{2}\left\{\mathbf{A}(\mathbf{r}, z) e^{i(kz-\omega t)} + c.c\right\} \tag{3.14}$$

where

$$E(\mathbf{q}, \mathbf{r}) = \frac{1}{2\pi}\left(\frac{\mu_o}{\epsilon_o n_0}\right)^{1/2} e^{(i\mathbf{q}\cdot\mathbf{r})} \tag{3.15}$$

and $k = \omega n_0/c$. The spatial frequency (or angular) distribution of the complex amplitude $A(\mathbf{r}, z)$ is given by $f(\mathbf{q}, r)$ where $\mathbf{r} = (x, y)$. Substituting Eq. (3.14) for the electric field into Eq. (3.4) and using the slowly-varying-envelope approximation yields the following equation for the propagation of the beam amplitude $A(\mathbf{r}, z)$:

$$\left(\frac{\partial}{\partial z} - \frac{i}{2k}\nabla_r{}^2\right) A(\mathbf{r}, z) = \frac{ik}{n_0}\delta n(\mathbf{r}, z)A(\mathbf{r}, z) \tag{3.16}$$

3.4 The photorefractive nonlinearity

When more than one pair of plane waves is present in the medium, we can use the two-wave mixing approximation to compute the index perturbation. This amounts to summing over the index gratings formed by all possible pairs of plane waves and can be written in integral form as [1]:

$$\delta n(\mathbf{r}, z) = \frac{1}{|A(\mathbf{r}, z)|^2 + I_d} \int d\mathbf{q}_1 \int d\mathbf{q}_2 f(\mathbf{q}_1, z) f^*(\mathbf{q}_2, z) E(\mathbf{q}_1, \mathbf{r}) \\ \mathrm{x} E^*(\mathbf{q}_2, \mathbf{r}) e^{i(\beta_{q_1} - \beta_{q_2})z} \hat{\delta n}(\mathbf{q}_1, \mathbf{q}_2) \tag{3.17}$$

In the most general case, $\hat{\delta n}(\mathbf{q}_1, \mathbf{q}_2)$ can be written in terms of its Fourier transform $g(\mathbf{p}, \mathbf{p}')$

$$\hat{\delta n}(\mathbf{q}_1, \mathbf{q}_2) = \int\int g(\mathbf{p}, \mathbf{p}') e^{-i(\mathbf{q}_1 \cdot \mathbf{p} + \mathbf{q}_2 \cdot \mathbf{p}')} d\mathbf{p} d\mathbf{p}' \tag{3.18}$$

Substituting into Eq. (3.17), and recalling the form of the electric field Eq. (3.14) yields

$$\delta n(\mathbf{r}, z) = \frac{1}{|A(\mathbf{r}, z)|^2 + I_d} \int\int A(\mathbf{r} - \mathbf{p}, z) A^*(\mathbf{r} + \mathbf{p}', z) g(\mathbf{p}, \mathbf{p}') d\mathbf{p} d\mathbf{p}' \tag{3.19}$$

Note that this form for the index perturbation reveals the nonlocal nature of the photorefractive effect.

Finally, we substitute the general form for the index perturbation into the nonlinear

wave equation Eq. (3.16):

$$\left(\frac{\partial}{\partial z} - \frac{i}{2k}\nabla_r{}^2\right) A(\mathbf{r},z) = \frac{ik}{n_0}\frac{1}{|A(\mathbf{r},z)|^2 + I_d}\int\int A(\mathbf{r}-\mathbf{p},z)A^*(\mathbf{r}+\mathbf{p}',z)$$
$$\mathrm{x}g(\mathbf{p},\mathbf{p}')d\mathbf{p}d\mathbf{p}' \qquad (3.20)$$

Within the two-wave mixing approximation, this equation describes the evolution of the amplitude of an optical beam in a photorefractive material. Although the task of solving this equation looks daunting, we will find that, following the methods of Segev *et al.*, we can make several simplifying assumptions to obtain a more manageable equation in the next chapter.

Chapter 4

In search of photorefractive solitons

Thus far we have derived an expression for the propagation of an optical beam in a photorefractive crystal. In this chapter, we will utilize the nonlinear photorefractive wave equation to describe the propagation of solitons in photorefractive crystals. Following the methods used by Segev *et al.*, we will simplify this equation and examine the fixed points of the resulting ordinary differential equation to determine the conditions under which bright and dark solitons exist.

4.1 The photorefractive soliton equation

At this point we need to consider how soliton formation occurs. As we expect, Eq. (3.20) shows that the beam experiences two effects as it propagates: those of diffraction and the nonlinear effect. Diffraction causes a uniform spreading of the beam, which can be thought of as a linear accumulation of phase in each spatial mode. To achieve soliton formation, we need the nonlinearity to provide a compensating effect. Earlier we showed that if $\hat{\delta n}(\mathbf{q}_1, \mathbf{q}_2)$ was real, then there was no energy exchange between modes and self-phase modulation

occurred. This is exactly what we need to get solitons: we want the amplitudes of each spatial mode to remain constant (no energy exchange) but for the phases of each mode to change linearly with propagation distance to balance diffraction. To attain a bright soliton we will need a self-focusing medium ($\hat{\delta n}(\mathbf{q}_1, \mathbf{q}_2) > 0$) to provide a linear decrease in phase. Alternately, for a dark soliton we need a self-defocusing medium ($\hat{\delta n}(\mathbf{q}_1, \mathbf{q}_2) < 0$) to provide linear phase increase.

With these conditions in mind, we substitute the spatial soliton ansatz

$$A(\mathbf{r}, z) = U(\mathbf{r})e^{i\gamma z} \tag{4.1}$$

into Eq. (3.20), where $U(\mathbf{r})$ is real and represents the transverse amplitude, and γ is the characteristic soliton propagation constant, which may be real or complex. This substitution yields the following integrodifferential equation for the amplitude $U(\mathbf{r})$:

$$\left(\gamma - \frac{1}{2k}\nabla_r{}^2\right) U(\mathbf{r}) = \frac{k}{n_0} \frac{U(\mathbf{r})}{U(\mathbf{r})^2 + I_d} \int\int U(\mathbf{r} - \mathbf{p})U(\mathbf{r} + \mathbf{p}')g(\mathbf{p}, \mathbf{p}')d\mathbf{p}d\mathbf{p}' \tag{4.2}$$

We can obtain an ordinary differential equation by Taylor expanding $U(\mathbf{r} \pm \mathbf{p})$ about $\mathbf{p} = 0$:

$$U(\mathbf{r} - \mathbf{p}) = U(\mathbf{r}) \pm \nabla_r U(\mathbf{r}) \cdot \mathbf{p} + \frac{1}{2}(\nabla_r \nabla_r U(\mathbf{r})) : \mathbf{pp} \pm \ldots \tag{4.3}$$

The smallness parameter associated with the Taylor expansion is d/l where d is the typical length scale of nonlocality, which is dictated by the form of $\hat{\delta n}(\mathbf{q}_1, \mathbf{q}_2)$, and l is the transverse beam width. This expansion will be justified later when we show that d is indeed small compared to l.

Because photorefractive materials are noncentrosymmetric, they lack cylindrical symmetry. This makes the full three-dimensional solution to this problem extremely difficult. If we restrict ourselves to one transverse dimension only, the equations become much more tractable.

4.2 Simplifying the two-dimensional photorefractive nonlinear wave equation

If we choose our single transverse dimension to be the x coordinate, and substitute the Taylor expansion Eq. (4.3) into the integrodifferential equation Eq. (4.2) we obtain the following [1]:

$$\left(\gamma - \frac{1}{2k}\frac{\partial^2}{\partial x^2}\right) U \approx \frac{k}{n_0}\frac{U}{U^2+I_d}\int\int\left\{U^2 + U\frac{\partial U}{\partial x}(\mathrm{p}'-\mathrm{p}) - \mathrm{pp}'\left(\frac{\partial U}{\partial x}\right)^2 + \frac{1}{2}U\frac{\partial^2 U}{\partial x^2}(\mathrm{p}^2+\mathrm{p}'^2) + \frac{1}{2}\frac{\partial U}{\partial x}\frac{\partial^2 U}{\partial x^2}\mathrm{pp}'(\mathrm{p}-\mathrm{p}')\right\} g(\mathrm{p},\mathrm{p}')\mathrm{dpdp}' \quad (4.4)$$

Now we define the quantities

$$\begin{aligned} I_{mn} &= \int \mathrm{dp}\int \mathrm{dp}' g(\mathrm{p},\mathrm{p}')\mathrm{p}^m \mathrm{p}'^n \\ &= e^{i(m+n)\frac{\pi}{2}}\frac{\partial^m}{\partial {q_1}^m}\frac{\partial^n}{\partial {q_2}^n}\hat{\delta n}(\mathbf{q}_1,\mathbf{q}_2)\Big|_{q_1=q_2=0} \end{aligned} \quad (4.5)$$

Expanding $\hat{\delta n}(\mathbf{q}_1,\mathbf{q}_2)$ as a power series in q_1 and q_2

$$\hat{\delta n}(\mathbf{q}_1,\mathbf{q}_2) = \sum_{m=0}^{\infty}\sum_{n=0}^{\infty} s_{mn} q_1^m q_2^n \quad (4.6)$$

then

$$I_{mn} = m!n!s_{mn}e^{i(m+n)\frac{\pi}{2}} \quad (4.7)$$

Because diffraction is a symmetric process, we need a symmetric process to balance it and therefore we require the symmmetry condition $\hat{\delta n}(\mathbf{q}_1,\mathbf{q}_2) = \hat{\delta n}(-\mathbf{q}_1,-\mathbf{q}_2)$. This means that $s_{mn} = 0$ if $m+n$ is odd. Moreover, the requirement that $\hat{\delta n}(\mathbf{q}_1,\mathbf{q}_2)$ be real implies that $s_{mn} = s^*_{mn}$ and therefore $I_{mn} = I^*_{mn}e^{i(m+n)\pi/2}$. Recalling that $U(x)$ is real and that the propagation constant γ is complex, we substitute $\gamma = \gamma_1 + i\gamma_2$ and $I_{mn} = I^{re}_{mn} + iI^{im}_{mn}$ into

Eq. (4.4) and equate real and imaginary parts:

$$\gamma_2 U = 0 \tag{4.8}$$

$$\gamma_1 U - \frac{1}{2k}\frac{d^2U}{dx^2} = \frac{kU}{n_0(U^2+I_d)}\left\{I_{00}^{re}U^2 - I_{11}^{re}\left(\frac{dU}{dx}\right)^2 + I_{20}^{re}U\frac{d^2U}{dx^2}\right\} \tag{4.9}$$

where we have used the relations $I_{20}^{im} = -I_{02}^{im}$, $I_{20}^{re} = I_{02}^{re}$ and I_{mm} is real for all m. Eq. (4.9) implies that $\gamma_2 = 0$ for all nonzero solutions.

To simplify our notation, we define the constants

$$a = \frac{1}{2k} + \frac{k}{n_0}I_{20}^{re} \tag{4.10}$$

$$b = \frac{k}{n1}I_{11} \tag{4.11}$$

$$e = \frac{k}{n_0}I_{00} \tag{4.12}$$

and Eq. (4.9) can be written more simply as

$$(\gamma - e)U^3 + \gamma I_d U - \left(aU^2 + \frac{I_d}{2k}\right)U'' + bU'^2U = 0 \tag{4.13}$$

where prime indicates the derivative with respect to the transverse coordinate x. When $I_d = 0$, this result reduces to that derived by Segev *et al.* [1]:

$$\gamma' U^2 - aUU'' + bU'^2 = 0 \tag{4.14}$$

where the two real propagation constants are related by $\gamma' = \gamma - e$.

4.3 Calculating the coefficients

The coefficients in the photorefractive soliton equation (Eq. (4.13)) are computed using the results derived previously for the space charge field in the two-wave mixing case. Recall that

soliton formation requires a real $\delta\hat{n}(\mathbf{q}_1, \mathbf{q}_2)$ to balance diffraction. From the definition of $\delta\hat{n}(\mathbf{q}_1, \mathbf{q}_2)$, given by Eq. (2.25), this can be satisfied under the condition that $|E_d| \ll |E_0| \ll |E_q|$. In deriving the propagation equation we have also assumed that the optical beam has small angular divergence (the paraxial approximation), which results in index gratings with large periods (or small K). Consequently the limiting field E_q is guaranteed to be large compared to $|E_d|$ (recall Eq. (2.17)) and we can satisfy $|E_d| \ll |E_0|$ by applying an appropriate bias field $|E_0|$. Under these conditions $\delta\hat{n}(\mathbf{q}_1, \mathbf{q}_2)$ is computed from Eq. (2.25) and Eq. (2.16). It is given by:

$$\begin{aligned} \delta\hat{n}(\mathbf{q}_1, \mathbf{q}_2) &\approx -\frac{1}{2} n_0^3 r_{33} Re(E_m) \\ &= \frac{1}{2} n_0^3 r_{33} E_0 \frac{1}{1 + \left(\frac{E_0 \epsilon_0 \epsilon_r}{e P_d}\right)^2 (q_1 - q_2)^2} \\ &= \frac{B}{1 + d^2 (q_1 - q_2)^2} \end{aligned} \tag{4.15}$$

where $B = 1/2 n_0^3 r_{33} E_0$ and $d = E_0 \epsilon_0 \epsilon_r / (e P_d)$, and $P_d = N_A(1 - N_A/N_D)$ is the ionized trap density. Here d is the smallness parameter that was mentioned when we introduced the Taylor expansion in Section 4.1. d represents the scale of nonlocality in the problem, or more intuitively, it is related to the mean distance L_0 that a carrier electron is transported by drift before it becomes re-trapped. This distance is much smaller than the width of the beam, making the Taylor expansion reasonable.

To compute a, b, and e we need the quantities I_{00}, I_{20}, and I_{11} which are defined by equation Eq. (4.7). The coefficients of the various powers of q_1 and q_2 are found by expanding Eq. (4.15), again assuming that d is small:

$$\delta\hat{n}(\mathbf{q}_1, \mathbf{q}_2) = B\left(1 - d^2 q_1^2 - d^2 q_2^2 + 2d^2 q_1 q_2 + \ldots\right) \tag{4.16}$$

This gives the following expressions for the coefficients:

$$\begin{aligned} a &= \frac{1}{2k} + \frac{2k}{n_0} B d^2 \\ b &= -\frac{2k}{n_0} B d^2 \\ e &= \frac{k}{n_0} B \end{aligned} \tag{4.17}$$

4.4 Phase-plane analysis

Now that we have a simplified equation for soliton propagation the true test comes. How do we determine the conditions under which bright and dark soliton solutions exist and are these conditions consistent with experiment?

The types of solutions to the photorefractive soliton equation (Eq. (4.13)) can be studied by examining the nature of the fixed points of the system. Consider Figure 4.1a) and c) which illustrate bright and dark soliton profiles. In the bright soliton case, the amplitude must vanish at the limits

$$\lim_{x \to \pm\infty} U \to 0$$

and reach some finite value at its peak. These conditions allow us to infer a possible phase diagram, as shown in Figure 4.1b). The path along the separatrix in the phase-plane diagram satisfies the bright soliton conditions and is the only trajectory that represents a bright soliton solution. Other solutions are oscillatory and unphysical because they require optical beams of infinite extent in the transverse direction. There are other phase-plane portraits that admit bright soliton solutions, but they involve codimension two fixed points. We will assume that codimension two fixed points do not occur in our model, and will later find that this assumption is justified.

Similarly the dark soliton phase-portrait, shown in Figure 4.1d), must satisfy the condition

$$\lim_{x\to\pm\infty} U \to constant$$

and U must pass through the origin. Again, the path along the separatrix in the phase-plane portrait has this necessary behaviour.

Now that we know the character of the phase-portraits we are looking for, the next step is to identify and classify the fixed points of the system.

4.5 The fixed points of the photorefractive soliton equation

To find the fixed points of Eq. (4.13), we define $Y = U'$ and rewrite the equation as two coupled nonlinear equations:

$$\begin{aligned} U' &= Y \\ Y' &= \frac{U}{aU^2 + \frac{I_d}{2k}}[(\gamma - e)U^2 + \gamma I_d + bY^2] \end{aligned} \tag{4.18}$$

There are three fixed points for this system of equations, which can be found using the condition $U' = Y' = 0$. One is the trivial fixed point $(U, Y) = (0, 0)$ and there are two nontrivial ones given by:

$$(U, Y) = \left(\pm\sqrt{\frac{\gamma I_d}{e - \gamma}}, 0\right) \tag{4.19}$$

The nontrivial fixed points exist under the following conditions:

$$\begin{aligned} (\gamma > 0): &\quad e > 0, \quad |\gamma| < |e|, I_d \neq 0 \\ (\gamma < 0): &\quad e < 0, \quad |\gamma| < |e|, I_d \neq 0 \end{aligned} \tag{4.20}$$

It is interesting that the nontrivial fixed points require nonzero dark irradiance I_d, a term that had been neglected in the original theory.

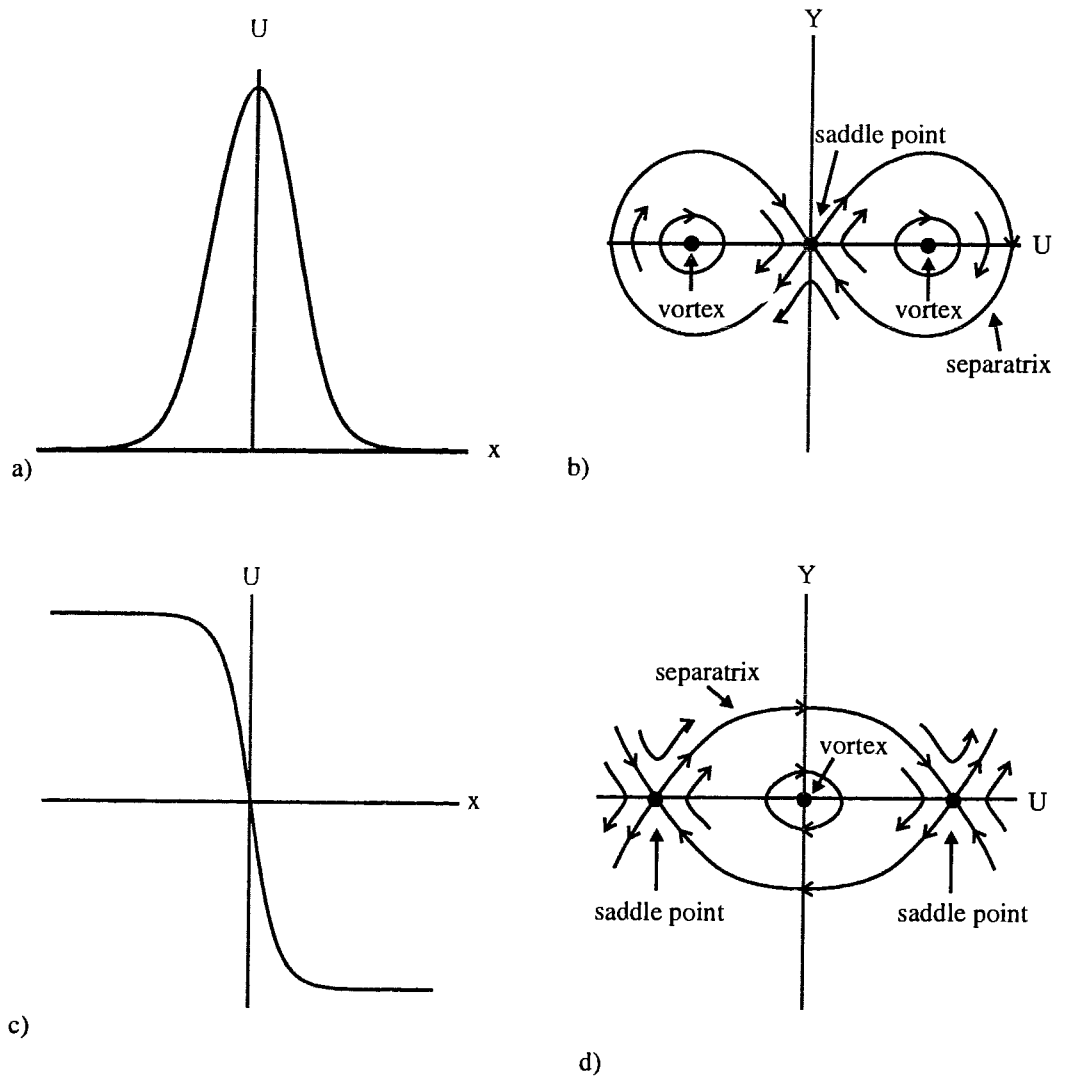

Figure 4.1: a) Amplitude profile of a bright soliton. b) Corresponding phase-portrait. The bright soliton occurs along the separatrix. c) Amplitude profile of a dark soliton. d) Corresponding phase-portrait. The dark soliton occurs along the separatrix.

The nature of each of the three fixed points can be determined by performing a linear stability calculation. This proceeds by studying the behaviour of the system near each fixed point. Let $U = U^* + u$ and $Y = Y^* + y$, where U^* and Y^* are the fixed point values of U and Y and u and y are small perturbations from U^* and Y^* respectively. Substituting into Eq. (4.18) and keeping terms to first order in u and y yields a set of linear equations of the form:

$$\begin{aligned} u' &= mu + ny \\ y' &= pu + qy \end{aligned} \tag{4.21}$$

These equations have the non-trival solution

$$\begin{aligned} u &= re^{\xi x} \\ y &= se^{\xi x} \end{aligned} \tag{4.22}$$

where the eigenvalues ξ are determined by the condition

$$\begin{vmatrix} m-\xi & n \\ p & q-\xi \end{vmatrix} = 0 \tag{4.23}$$

The behaviour of phase space trajectories near the fixed points can be deduced from the eigenvalues. In a set of two equations like this one, ξ has two possible roots. If both roots are imaginary, trajectories will circle the fixed point, and the fixed point is said to be a vortex. If both roots are real, with one positive and the other negative, the fixed point is a saddle point. Both of these types of fixed points were illustrated earlier in Figure 4.1. They are the only two types that arise from our set of equations but the interested reader is referred to [30] and [31] for an extensive study of the subject. The results of the linearization are summarized in Table 4.1. With knowledge of the eigenvalues, the corresponding fixed

Fixed Point (U^*, Y^*)	m	n	p	q	ξ
$(0,0)$	0	1	$2k\gamma$	0	$\pm\sqrt{2k\gamma}$
$\left(\sqrt{\frac{\gamma I_d}{e-\gamma}}, 0\right)$	0	1	$-\frac{4k\gamma(e-\gamma)}{(2ka-1)\gamma+e}$	0	$\pm\sqrt{-\frac{4k\gamma(e-\gamma)}{(2ka-1)\gamma+e}}$
$\left(-\sqrt{\frac{\gamma I_d}{e-\gamma}}, 0\right)$	0	1	$-\frac{4k\gamma(e-\gamma)}{(2ka-1)\gamma+e}$	0	$\pm\sqrt{-\frac{4k\gamma(e-\gamma)}{(2ka-1)\gamma+e}}$

Table 4.1: Linear stability results for the three fixed points of Eq. (4.18).

Fixed Point (U^*, Y^*)		Character of fixed point
$(0,0)$	$\gamma > 0$	saddle
	$\gamma < 0$	vortex
$\left(\pm\sqrt{\frac{\gamma I_d}{e-\gamma}}, 0\right)$	$a > 0, e > 0, \gamma > 0$	vortex
	$a > 0, e > 0, \gamma < 0$	saddle
	$a < 0, e < 0, \gamma < \frac{-e}{2ka-1}$	vortex
	$a < 0, e < 0, \frac{-e}{2ka-1} < \gamma < 0$	saddle

Table 4.2: The fixed points and the conditions determining their character.

points can be classified. These classifications are given in Table 4.2. Note here that the case $a < 0, e > 0$ was not mentioned because the definitions given in Eq. (4.12) imply that $a > 0$. The existence criteria Eq. (4.20) for the non-trivial fixed points have been included.

Comparison of Table 4.2 with Figure 4.1b) and Figure 4.1d) give the necessary conditions to obtain the two types of soliton solutions. For bright solitons, we combine conditions that provide a saddle-point at the origin and two vortices at the nontrivial fixed points to obtain:

$$\textit{bright solitons} : e > 0, \gamma > 0 \tag{4.24}$$

Conversely, for dark solitons we combine conditions that provide a vortex at the origin and

two saddle-points at the nontrivial fixed points to obtain:

$$dark\ solitons: a \geq 0, \epsilon < 0, \gamma < 0 \quad \text{or} \quad a < 0, \epsilon < 0, \frac{-\epsilon}{2ka-1} < \gamma < 0 \tag{4.25}$$

This is interesting because it suggests that to switch from bright to dark solitons, the sign of ϵ must change. From the definition of ϵ this corresponds to changing the sign of the bias field relative to the c-axis of the crystal. This fact has been confirmed experimentally in [4] and [5] and corresponds to changing the medium from self-focusing ($\epsilon > 0, E_0 > 0$) to self-defocusing ($\epsilon < 0, E_0 < 0$).

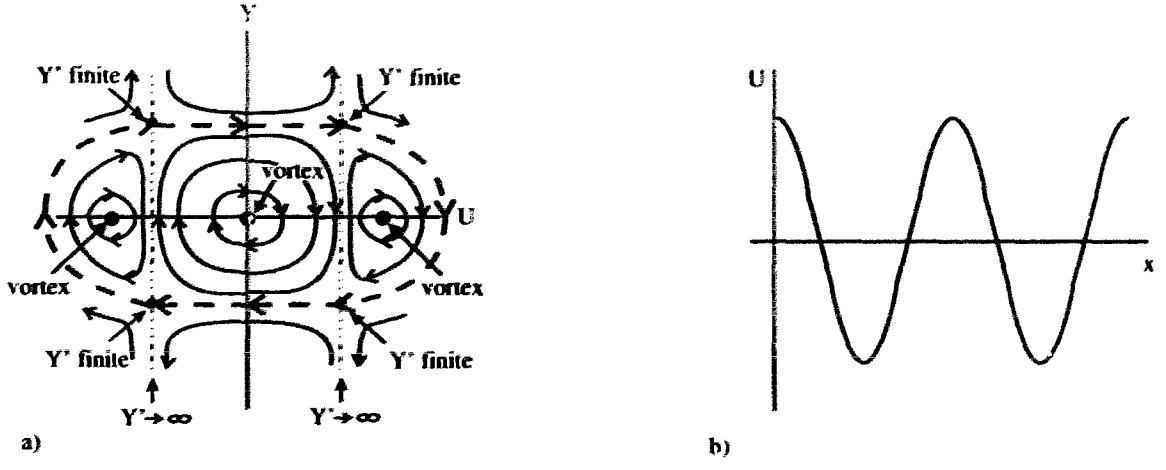

Figure 4.2: a) Phase-portrait when all three fixed points are vortices. The phase-plane is divided into three sections by the lines along which Y' is infinite. These lines are defined by the equation $aU^2 + \frac{I_d}{2k} = 0$. There are four points at which Y' is finite and these occur when $(\gamma - \epsilon)U^2 + \gamma I_d + bY^2 = 0$. The only path through phase space that passes from one section to the next must pass through these points (shown by the thick dashed line). b) The amplitude $U(x)$ for the dashed line trajectory in a). The solution is periodic and therefore unphysical since it cannot represent a single optical beam propagating through the photorefractive material.

Another interesting result can be derived from the linear stability analysis. When the medium is self-defocusing, the parameter a has the capability of changing sign. When this

occurs the fixed points are either in the dark soliton configuration, or they are all vortices, as shown in Figure 4.2. In this case, the phase-plane is divided into three sections by the lines along which $Y' \to \infty$. Note that each of these lines has two points at which Y' is finite. Thus a possible solution consists of a path in phase space that passes through these well defined points as shown. This solution is not interesting as a solitary wave candidate because it does begin or end at any fixed points. It is rather an oscillatory solution, requiring an infinite extent in the x direction. Dark solitons are only possible when the $Y' \to \infty$ lines lie outside the nontrivial fixed points, and we recover the familiar dark soliton fixed point configuration. If we assume that the peak intensity of the soliton (given by U^{*2}) is approximately equal to the peak intensity I_{max} of the input beam, we can obtain a condition on the magnitude of the bias field applied to the crystal to achieve dark solitons:

$$|E_0| < \left(\frac{(I_{max} + I_d)}{I_{max}} \frac{\lambda^2 e^2 P_d^2}{8\pi^2 n_0^4 \epsilon_o^2 \epsilon_r^2 r_{33}} \right)^{1/3} \tag{4.26}$$

There has only been one experimental paper reporting photorefractive nonlocal dark solitons, and it contains no evidence to support or contradict this condition [4].

4.6 Comparison with experiment

In the previous section we demonstrated that the photorefractive soliton equation had the necessary characteristics to admit both bright and dark soliton solutions. In this section realistic parameters will be used to show that these solitons do exist under conditions consistent with experiment. The following parameters are reported in [5] and [4] for experiments in SBN: $\lambda = 0.5\ \mu$m, $n_0 = 2.35$, $r_{33} = 2.24\text{x}10^{-4}\ \mu$m/V, $\epsilon_r = 1100$, $P_d = 4\text{x}10^4\ \mu\text{m}^{-3}$, and $|E_0| = 5\text{x}10^5$ V/m, which lead to the coefficient values listed in Table 4.3. The dark irradiance I_d is estimated to be $\approx$ 10 - 100 mW/cm^2 [32][4].

Figure 4.3 shows the phase-portraits for the bright and dark cases using the parameters

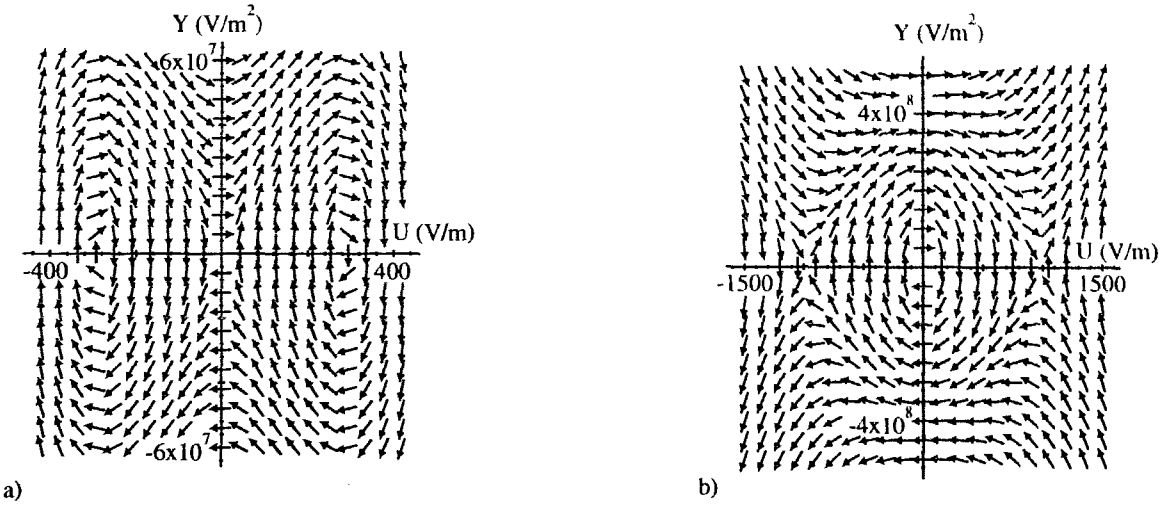

Figure 4.3: a) Phase-portrait for the bright soliton case ($\gamma = 1.9x10^{-3}$). b) Corresponding dark soliton phase-portrait ($\gamma = -6.85x10^{-3}$).

listed in Table 4.3. The corresponding amplitude and intensity profiles for the bright and dark cases are shown in Figure 4.4a),c) and Figure 4.4b),d) respectively. By choosing γ, soliton solutions can be found to correspond with the power of the optical beam. This is particularly easy in the dark soliton case, since U^* represents the peak amplitude, and γ can then be found from Eq. (4.19):

$$\gamma = \frac{eU^{*2}}{I_d + U^{*2}} \tag{4.27}$$

The bright soliton case requires a bit of guesswork. Experimentally, bright solitons have been generated for intensities in the range 0.05 - 78.5 W/cm^2, which corresponds to electric field values of $\approx$ 400 - 1.6x10^4 V/m. Note that the lowest intensity value is not much greater than the estimated dark irradiance (10 - 100 mW/cm^2). Dark solitons have been observed for intensities of 0.3 - 30 W/cm^2, or electric field values of $\approx$ 1x10^3 - 1x10^4 V/m [4]. The photorefractive soliton equation yields both bright and dark soliton solutions for both these

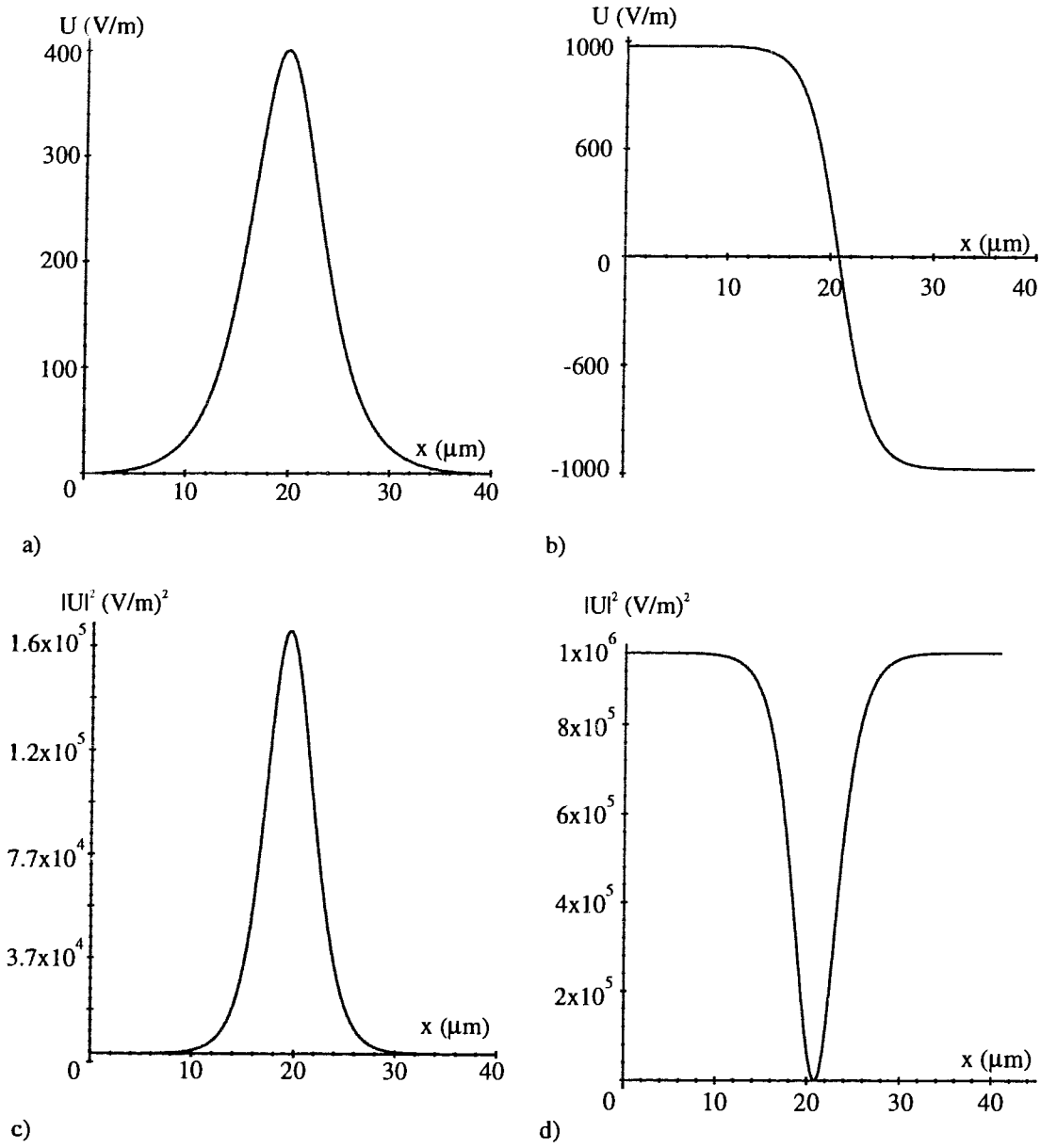

Figure 4.4: a) Amplitude profile of a bright soliton ($\gamma = 1.9x10^{-3}$). b) Amplitude profile of a dark soliton ($\gamma = -6.85x10^{-3}$). c) Corresponding bright soliton intensity profile (peak of 0.05 W/cm^2). d) Corresponding dark soliton intensity profile (peak of 0.3 W/cm^2).

Soliton Type	Bright	Dark
E_0(V/m)	5.0x10^5	-5.0x10^5
B	7.27 x 10^{-4}	-7.27 x 10^{-4}
d (μm)	7.59x10^{-1}	-7.59x10^{-1}
a (μm)	2.75x10^{-2}	6.41x10^{-3}
b (μm)	-1.05x10^{-2}	1.05x10^{-2}
e (μm^{-1})	9.13x10^{-3}	-9.13x10^{-3}

Table 4.3: Experimental parameters from [4][5].

ranges of electric field. Two examples are shown in Figure 4.4.

Using the parameters in Table 4.3, we predict the following condition on the bias field when the incident intensity is large compared to I_d:

$$|E_0| < 5.85\text{x}10^5 \text{ V/m} \tag{4.28}$$

When the incident intensity is comparable to I_d the maximum field condition can be derived from Eq. (4.26).

4.7 The Segev equation

Earlier when we derived the photorefractive soliton equation, we mentioned that if the dark irradiance I_d was neglected, we obtained Eq. (4.14) derived by Segev *et al.* [1]. It is interesting to compare the differences between these equations to understand how they permit different solutions.

We begin by looking at the fixed points of the Segev equation. Making the substitution

$Y = U'$ yields the following set of coupled equations

$$\begin{aligned} U' &= Y \\ Y' &= \frac{1}{a}\left(\gamma' U + b\frac{Y^2}{U}\right) \end{aligned} \tag{4.29}$$

Eq. (4.29) has a single fixed point at the origin (as well as fixed points at $\pm\infty$). The standard stability analysis used previously cannot be applied here because it is readily shown that the system has two zero eigenvalues. However, the general character of the fixed point is revealed by plotting the phase-portrait (see Figure 4.5). Unlike the $(0,0)$ fixed point examined earlier, this one has the character of both a saddle node and a vortex and is a codimension two fixed point [30]. The system permits an infinite number of bright soliton solutions instead of a single solution for each set of parameters (recall the single separatrix in Figure 4.1b)). The Segev equation does not permit dark soliton solutions. This is

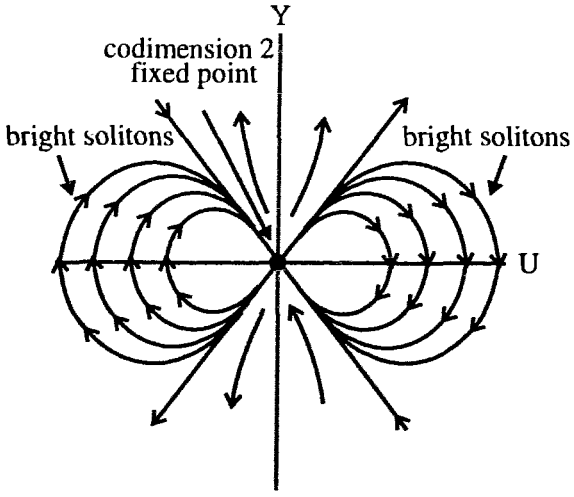

Figure 4.5: Phase-plane for bright soliton solutions of the Segev equation.

apparent because there is a singularity at $U = 0, Y \neq 0$. The Segev equation can be solved

exactly for bright solitons solutions. They are found to have the following form:

$$U(x) = U_0[\mathrm{sech}(\alpha x)]^D \tag{4.30}$$

where $D = a/(b-a), \alpha = \sqrt{\gamma(a-b)}/a$. The constants a and b are defined in Eq. (4.12). The arbitrary constant U_0 reflects the behaviour seen in the phase-plane that permits an infinite number of solutions for a single set of parameters. The requirement $D > 0$ guarantees that the boundary conditions at $x \to \pm\infty$ are satisfied. This yields an upper and lower bound on the applied electric field; for bright solitons in SBN this condition is

$$\left(\frac{(\lambda e P_d)^2}{16\pi^2 r_{33} n_0^4 \epsilon_o^2 \epsilon_r^2}\right)^{1/3} < |E_0| < \left(\frac{(\lambda e P_d)^2}{8\pi^2 r_{33} n_0^4 \epsilon_o^2 \epsilon_r^2}\right)^{1/3} \tag{4.31}$$

For the parameters in Table 4.2 this condition reduces to

$$-5.85\text{x}10^5\text{V/m} < E_0 < -4.60\text{x}10^5\text{V/m} \tag{4.32}$$

The polarity of the electric field is not consistent with experiment. We have demonstrated that bright solitons require $E_0 > 0$ or equivalently $\delta n > 0$, which corresponds to self-focusing [2][4], and this has been verifed experimentally [19]. Segev's equation predicts the opposite: that bright solitons occur when the medium is self-defocusing, and dark solitons occur when the medium is self-focusing. One experimental paper reports reasonable agreement with the bounds set on the magnitude of the bias field by the Segev prediction [2].

4.8 The small modulation approximation

Our theory relies on the small modulation approximation, which allows us to ignore all but the first Fourier component in deriving the space-charge field inside the crystal. Recall that this assumption requires that there be high conductivity in all regions of the crystal.

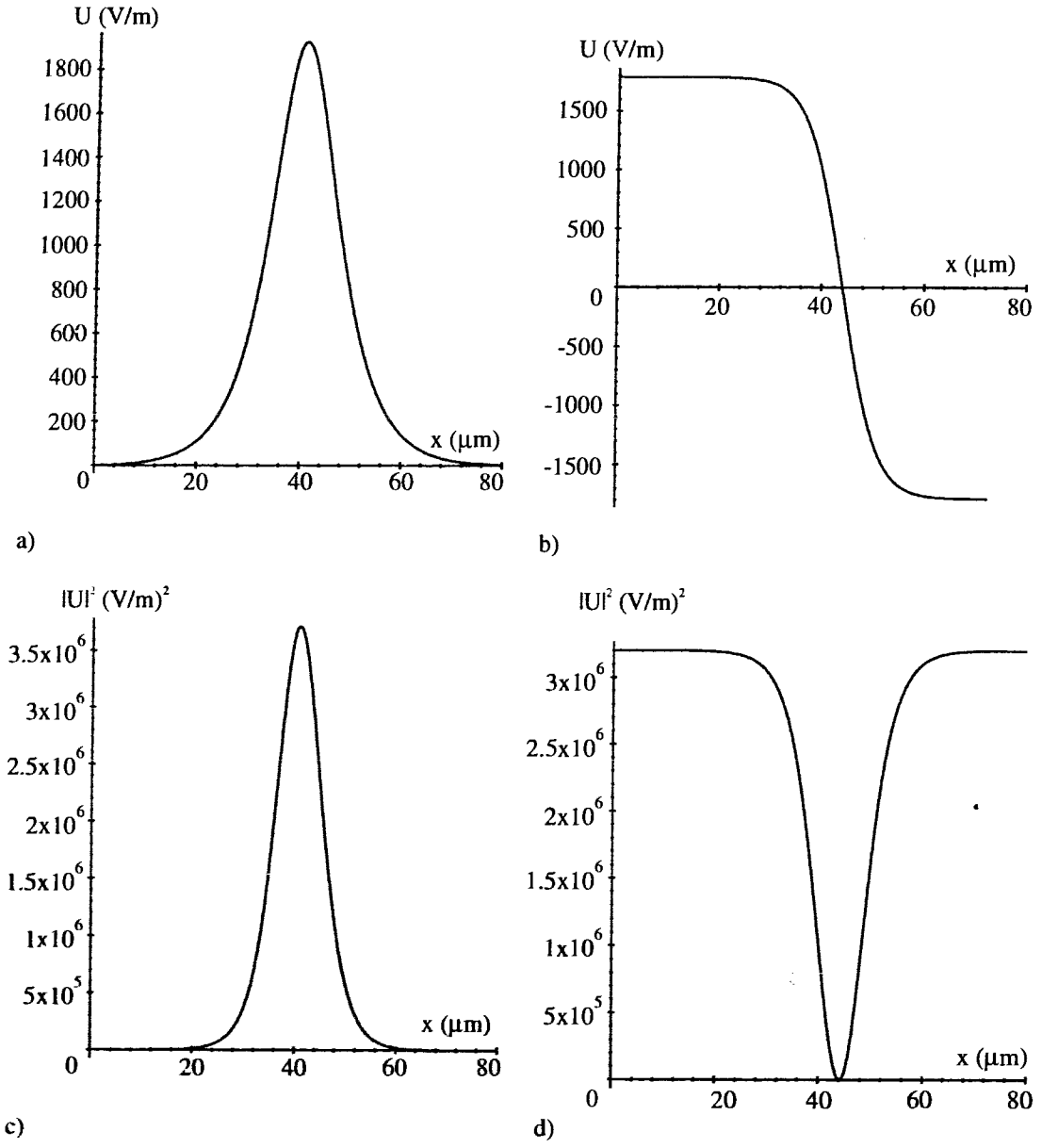

Figure 4.6: a) Amplitude profile of a bright soliton ($\gamma = 5\text{x}10^{-4}$). b) Amplitude profile of a dark soliton ($\gamma = -8.23\text{x}10^{-4}$). c) Corresponding bright soliton intensity profile (peak of 1.2 W/cm^2). d) Corresponding dark soliton intensity profile (peak of 1 W/cm^2). I_b=10 W/cm^2 and I_d=10 mW/cm^2.

Segev's method ignores this requirement entirely, which makes his analysis inaccurate in regions of low intensity (the edges of the beam), or when the incident intensity is of the same order as the dark irradiance. Our analysis is somewhat better. By including the dark irradiance we have removed the unphysical divergence from the Segev equation. However, we have still neglected to require a constant background illumination that is needed to make our approximations fully valid when I_0 is large compared to I_d. This was done largely to compare the theory with experiments, which do not use background illumination. Like Segev's method, our analysis is poorest in regions of low intensity; near the beam edges for bright solitons, or the centre of dark solitons. When the optical beam irradiance is of the same order as the dark irradiance, our analysis is valid for all parts of the beam.

We can extend our method to include the background illumination by adding this term to the dark irradiance in the denominator of Eq. (3.20), and adjusting the average index of refraction n_0 to account for the constant internal electric field that would be created in the crystal. What this does is essentially redefine what we mean by 'dark', so that conductivity that was originally due to thermal effects now includes photoconductivity from the background illumination. The rest of the analysis proceeds as before. The phase plane analysis and conditions for soliton formation are the same, with the term I_d being replaced by $I_d + I_b$ where I_b is the background illumination. Figure 4.6 shows bright and dark soliton profiles for $I_b = 10$ W/cm^2 and $I_d = 10$ mW/cm^2.

4.9 Other assumptions

To obtain the photorefractive soliton equation we have made several additional assumptions. We began by deriving the change in refractive index for two plane waves in the medium. We ignored the photovoltaic effect, which is valid for materials such as SBN and most other photorefractive crystals that have negligible photovoltaic properties. In deriving an expression for optical beam propagation in photorefractive materials we assumed that the

beam had small angular divergence which allowed us to neglect second derivatives in z. This is a frequently used approximation which can be easily satisfied experimentally [33].

We have neglected absorption in our model of photorefraction. Experimental studies of nonlocal solitons have not reported diminishing soliton amplitude due to absorption. This merits further investigation because absorption coefficients for SBN suggest that for propagation distances as large as 5mm, absorption effects should play a role [23].

We have restricted our analysis to one transverse dimension to simplify the mathematics of finding soliton solutions. In materials such as SBN which have one dominant electro-optic coefficient, this has been shown to be a reasonable approximation because coupling along one transverse direction is much stronger than the coupling along the other. By choosing to polarize the optical beam along the c-axis, the largest coupling occurs along this direction, making coupling contributions from the other transverse dimension negligible.

Our final assumption was that the scale of nonlocality d was small compared to the soliton width l. Taking our d value from Table 4.3 and estimating $l \approx 40\mu$m yields $d/l \approx 0.019$. Recall that we have kept to second order in this parameter. From Eq. (4.16), we see that there are no odd orders in d so that the next highest order is fourth order, which is extremely small ($\approx 1\text{x}10^{-7}$), making this a reasonable assumption. One could avoid the Taylor expansion altogether and numerically integrate Eq. (3.20) by a method such as the 'split step Fourier method' [33]. However, it is doubtful that much would be gained in the analysis given here for SBN because the terms we have neglected are so small.

Chapter 5

Stability of nonlocal solitons

Experimentally, nonlocal solitons have been shown to be stable despite the index inhomogeneities that are always present in photorefractive crystals. They have also been observed to evolve from an arbitrary input waveform [2][13]. This chapter presents a theoretical stability argument adapted from one developed by Segev *et al.* [13] to suit both bright and dark solitons of the type discussed previously. The evolution properties of the solitons will not be addressed.

The analysis begins by recalling the paraxial nonlinear wave equation developed previously:

$$\left(\frac{\partial}{\partial z} - \frac{i}{2k}\frac{\partial^2}{\partial x^2}\right) A(x,z) = \frac{ik}{n_0}\delta n(x,z)A(x,z) \tag{5.1}$$

where, as before, we are restricting the analysis to two dimensions. A soliton solution to this equation has the form

$$A(x,z) = U(x)e^{i\gamma z} \tag{5.2}$$

Now let us assume the presence of an index perturbation that causes a deviation from the soliton solution so that the field amplitude now has the form

$$A(x,z) = U^{(0)}(x)e^{i\gamma z} + U^{(1)}(x,z) \tag{5.3}$$

where $U^{(1)}$ represents the perturbation and we require $|U^{(1)}|^2 \ll |U^{(0)}|^2$. As before, the light induced photorefractive change in index is assumed to be real, (but permitting uniform absorption) so that $\delta n(x,z) = \delta n^*(x,z)$. Multiplying Eq. (5.1) by A^* and adding its complex conjugate yields the equation:

$$\frac{\partial}{\partial z}(AA^*) + \frac{i}{2k}\left(A\frac{\partial^2 A^*}{\partial x^2} - A^*\frac{\partial^2 A}{\partial x^2}\right) = 0 \tag{5.4}$$

This equation is an expression of conservation of energy. Substituting the perturbed solution Eq. (5.3) into Eq. (5.4) and keeping to first order in $U^{(1)}$ yields

$$\begin{aligned}&\left\{U^{(0)}\left[U_z^{(1)*} + i\gamma U^{(1)*}\right] + \frac{i}{2k}\left[U^{(0)}U_{xx}^{(1)*} - U^{(1)*}U_{xx}^{(0)}\right]\right\}e^{i\gamma z}\\ &+\left\{U^{(0)}\left[U_z^{(1)} - i\gamma U^{(1)}\right] + \frac{i}{2k}\left[U^{(0)}U_{xx}^{(1)} - U^{(1)}U_{xx}^{(0)}\right]\right\}e^{-i\gamma z} = 0\end{aligned} \tag{5.5}$$

Grouping terms with identical exponential arguments gives the equation

$$\frac{U_z^{(1)}}{U^{(1)}} - i\gamma + \frac{i}{2k}\left[\frac{U_{xx}^{(0)}}{U^{(0)}} - \frac{U_{xx}^{(1)}}{U^{(1)}}\right] = 0 \tag{5.6}$$

Let us assume that the perturbation takes place on a length scale l_p which is small compared to the soliton width l, and larger or of the same order as the wavelength of light λ ($l \gg l_p \geq \lambda$). The paraxial approximation requires that the longitudinal scale l_z of $U^{(1)}$ be larger than l_p, but it may still be small relative to the soliton size. In addition, it was shown previously that soliton solutions occur for $|\gamma| < |e|$, where $e \propto k$. This implies that at most $\gamma \approx 1/\lambda$. Comparing the relative magnitude of the various terms in Eq. (5.6):

$$\frac{U_z^{(1)}}{U^{(1)}} \approx \frac{1}{l_z},\quad \gamma \approx \frac{1}{\lambda},\quad \frac{U_{xx}^{(1)}}{kU^{(1)}} \approx \frac{\lambda}{l_p^2},\quad \frac{U_{xx}^{(0)}}{kU^{(0)}} \approx \frac{\lambda}{l^2} \tag{5.7}$$

Thus we are justified in neglecting the third term in Eq. (5.6) to obtain a simplified equation

governing the propagation of the perturbation:

$$U_z^{(1)} - i\gamma U^{(1)} - \frac{i}{2k} U_{xx}^{(1)} = 0 \tag{5.8}$$

This equation reveals that $U^{(1)}$ propagates almost independently of the soliton solution $U^{(0)}$. If we make the transformation

$$U(x,z) = e^{i\gamma z} V(x,z), \tag{5.9}$$

then the second term is removed and the equation has the form:

$$U_z^{(1)} - \frac{i}{2k} U_{xx}^{(1)} = 0 \tag{5.10}$$

This equation, along with its accompanying conservation of energy relation

$$\frac{d}{dz} \int_{-\infty}^{\infty} |U^{(1)}|^2 dx = 0 \tag{5.11}$$

implies that the perturbation remains small in magnitude and eventually diffracts away as it propagates. This is apparent because Eq. (5.10) has the same form as the paraxial wave equation with no nonlinear term to balance the effect of diffraction. Thus the perturbation dies off and we can say that for perturbations that are small relative to the soliton size, the soliton is relatively stable. This conclusion is in agreement with an experimental study done by Duree *et al.* [14] for bright solitons in SBN. No perturbing studies of this kind have been done for dark solitons.

Chapter 6

Conclusions

Photorefractive nonlocal solitons of the bright and dark type have been observed experimentally. They occur when the spreading effect of diffraction is balanced by the self-focusing or self-defocusing effect of the phase coupling between spatial modes of the input beam. These solitons are thought to be potentially useful in all-optical switching devices because they can be generated at very low light intensities. The original theory of nonlocal soliton formation proposed by Segev *et al.* [1] accounted only for the existence of bright solitons. It also predicted that these solitons could be found when the medium was self-defocusing, a fact that experiment has shown to be incorrect. Using the same two-wave mixing formalism as the original theory, we have derived an equation to describe the propagation of solitons in photorefractive materials. This equation includes the dark irradiance in the calculation of the change in index of refraction, and thus removes the unphysical divergence that was present in Segev's equation under zero incident intensity. Our theory predicts that a nonzero dark irradiance is essential for nonlocal soliton formation. A possible method for testing this prediction would be to lower the crystal temperature, and thus the dark irradiance, and observe what effect this has on bright and dark nonlocal soliton formation.

By analyzing the fixed points of the equation, we found both dark and bright soliton solutions and conditions for their existence. We demonstrated that bright soliton solutions

require the polarity of the bias field to be such that the medium is self-focusing. Conversely, dark solitons require self-defocusing which is achieved by switching the polarity of the bias field. Both of these predictions have been verified experimentally. There is no available experimental evidence to support the maximum bias field condition that we obtained for dark solitons. We have also shown that nonlocal solitons are stable to index perturbations that are small compared to the size of the soliton. This fact has been experimentally confirmed.

Qualitatively, our theory does a good job of predicting the type of behaviour that has been observed in soliton experiments. However, caution should be used when comparing our results directly with those of experiment. The reason for this prudence is that all of the experiments to date have used zero background illumination, which is inconsistent with the conditions necessary for the small modulation approximation. This means that at best our theory can describe the high intensity portions of the beam, unless the beam irradiance is comparable to the dark irradiance. If the incident intensity is large compared to I_d, our theory is more appropriately applied with the presence of a constant background illumination. It would be interesting to see how well our theory corroborates experiments done under such conditions.

A complete description of nonlocal solitons in photorefractive materials is still lacking. To date, the theory accounts only for self-trapping in one dimension and does not explain the experimental observations of soliton formation along both transverse directions. Analysis has been restricted to materials such as SBN which have one dominant electro-optic coefficient, allowing the approximation that coupling between tranverse modes is small. A full three dimensional treatment has not been attempted here because the lack of cylindrical symmetry in the problem makes solving the photorefractive nonlinear wave equation very difficult. Any future progress in this area will likely rely on numerical studies of the full three dimensional problem. Other questions that remain unanswered include soliton collisions and the evolution properties of nonlocal solitons from arbitrary input beams. In

addition, the effect of absorption on nonlocal soliton formation needs investigation. Nevertheless, the basic effect of nonlocal soliton formation seems to be understood. We now have a theory which qualitatively predicts bright and dark solitons under conditions consistent with experiment.

Bibliography

[1] M. Segev, B.Crosignani, and A. Yariv. Spatial solitons in photorefractive media. *Phys. Rev. Lett.*, 68:923, 1992.

[2] G. Duree, J. Shultz, G. Salamo, M. Segev, A. Yariv, B.Crosignani, P. Di Porto, E. Sharp, and R. Neurgaonkar. Observation of self-trapping of an optical beam due to the photorefractive effect. *Phys. Rev. Lett.*, 71:533, 1993.

[3] P. Gunter and J. Huignard. *Photorefractive Materials and Their Applications I.* Springer Verlag, 1988.

[4] G. Duree, M. Morin, G. Salamo, M. Segev, B.Crosignani, P. Di Porto, E. Sharp, and A. Yariv. Dark photorefractive spatial solitons and photorefractive vortex solitons. *Phys. Rev. Lett.*, 74:1978, 1995.

[5] B. Crosignani, M. Segev, P. Di Porto, A. Yariv, and G. Salamo. Self-trapping of optical beams in photorefractive media. *J. Opt. Soc. Am. B*, 10:446, 1993.

[6] M. Remoissenet. *Waves Called Solitons.* Springer-Verlag, 1994.

[7] A. Hasegawa. *Optical Solitons in Fibers.* Springer-Verlag, 1990.

[8] C. Gardner, J. Greene, M. Kruskal, and R. Muira. Method for solving the Korteweg de Vries equation. *Phys.Rev.Lett.*, 19:1095, 1967.

[9] A. Davydov. *Solitons in Molecular Systems.* Reidel, 1985.

[10] S. Antipov, M.Nezlin, E. Snezhkin, and A. Trubnikov. Rossby autosoliton and stationary model of the Jovian Great Red Spot. *Science*, 323:238, 1986.

[11] R. H. Enns, D. E. Edmundson, S. S. Rangnekar, and A. E. Kaplan. Optical switching between bistable soliton states: a theoretical review. *Opt. and Quantum Electron.*, 24:S1295, 1992.

[12] M. Segev, Y. Ophir, and B. Fischer. Photorefractive self-defocusing. *App. Phys. Lett.*, 56:1086, 1990.

[13] M. Segev, B.Crosignani, P. Di Porto, A. Yariv, G. Duree, G. Salamo, and E. Sharp. Stability of photorefractive spatial solitons. *Opt. Lett.*, 19:1296, 1994.

[14] G. Duree, G. Salamo, M. Segev, A. Yariv, B.Crosignani, P. Di Porto, and E. Sharp. Dimensionality and size of photorefractive spatial solitons. *Opt. Lett.*, 19:1195, 1994.

[15] M. Castillo, J. Sanchez-Mondragon, S. Stepanov, M. Klein, and B. Wechsler. (1+1)-dimension dark spatial solitons in photorefractive $Bi_{12}TiO_{20}$ crystal. *Opt. Commun.*, 118:515, 1995.

[16] P. Yeh. *Introduction to Photorefractive Nonlinear Optics.* John Wiley & Sons, 1993.

[17] G. Valley, M. Segev, B. Crosignani, A. Yariv, M. Fejer, and M. Bashaw. Dark and bright photovoltaic spatial solitons. *Phys. Rev. A*, 50:4457, 1994.

[18] M. Taya, M. Bashaw, M. Fejer, M. Segev, and G. Valley. Observation of dark photovoltaic spatial solitons. *Phys. Rev. A*, 52:3095, 1995.

[19] M. Segev, G. Valley, B.Crosignani, P. Di Porto, and A. Yariv. Steady-state spatial screening solitons in photorefractive materials with external applied field. *Phys. Rev. Lett.*, 73:3211, 1994.

[20] D. Christodoulides and M. Carvalho. Bright, dark, and gray spatial soliton states in photorefractive media. *J. Opt. Soc. Am. B*, 12:1628, 1995.

[21] M. Carvalho, S. Singh, and D. Christodoulides. Self-deflection of steady-state bright spatial solitons in biased photorefractive crystals. *Opt. Commun.*, 120:311, 1995.

[22] M. Shih, P. Leach, M. Segev, M. Garrett, G. Salamo, and G. Valley. Two-dimensional steady-state photorefractive screening solitons. *Opt. Lett.*, 21:324, 1996.

[23] M. Petrov, S. Stepanov, and A. Khomenko. *Photorefractive Crystals in Coherent Optical Systems.* Springer-Verlag, 1991.

[24] C. Kittel. *Introduction to Solid State Physics.* John Wiley & Sons, Inc., 1986.

[25] N. Kukhtarev, V. Markov, S. Odulov, M. Soskin, and V.Vinetskii. Holographic storage in electrooptic crystals. I steady state. *Ferroelectrics*, 22:949, 1979.

[26] N. Kukhtarev, V. Markov, S. Odulov, M. Soskin, and V.Vinetskii. Holographic storage in electrooptic crystals. II beam coupling-light amplification. *Ferroelectrics*, 22:961, 1979.

[27] M. Moharam, T. Gaylord, and R. Magnusson. Holographic grating formation in photorefractive crystals with arbitrary electron transport lengths. *J. Appl. Phys.*, 50:5642, 1979.

[28] A. Mamaev and V.Shkunov. Interaction of counterpropagating waves and phase self-conjugation in a $BaTiO_3$ crystal. *Soviet Journal of Quantum Electronics*, 19:1199, 1989.

[29] D. Christodoulides and M. Carvalho. Compression, self-bending, and collapse of gaussian beams in photorefractive crystals. *Opt. Lett.*, 19:1714, 1994.

[30] J. Guckenheimer and P. Holmes. *Nonlinear Oscillations, Dynamical Systems, and Bifurcations of Vector Fields.* Springer-Verlag, 1983.

[31] P. Manneville. *Dissipative Structures and Weak Turbulence.* Academic Press, Inc., 1990.

[32] S. Singh and D. Christodoulides. Evolution of spatial optical solitons in biased photorefractive media under steady-state conditions. *Opt. Commun.*, 118:469, 1995.

[33] G. Agrawal. *Nonlinear Fiber Optics.* Academic Press, Inc., 1989.